



1 **Decadal ocean observations in the Northwestern** 2 **Mediterranean: insights from the MOOSE-GE cruises**

3 Laurent Coppola¹, Anthony Bosse², Thibaut Wagener², Dominique Lefevre², Magali Lescot²,
4 François Carlotti², Fabien Lombard³, Lionel Guidi³, Fabrice Not⁴, Xavier Durrieu de Madron⁵,
5 Pascal Conan¹, Mireille Pujo-Pay⁶, Caroline Ulses⁷, Samuel Somot⁸, Claude Estournel⁷, Emilie
6 Diamond Riquier⁴, Céline Laus⁴, Nathalie Leblond⁹, Matthieu Labaste¹⁰, Patrice Bretel¹⁰, Melek
7 Golbol¹⁰, Stephane Kunesch⁵, Jennifer Sola⁵, Laure Chirurgien², Sandra Nunige², Sarah Romac⁴,
8 Pierre Testor¹⁰

9
10 ¹ Sorbonne Université, CNRS, OSU STAMAR, UAR2017, 4 place Jussieu, 75252 Paris Cedex 05, France.

11 ² Aix Marseille Université, CNRS, IRD, Toulon Université, MIO, Marseille, France.

12 ³ Sorbonne Université, CNRS, Laboratoire d'Océanographie de Villefranche (LOV), 06230 Villefranche-sur-Mer,
13 France.

14 ⁴ Sorbonne Université, CNRS, Station Biologique de Roscoff, AD2M, 29680 Roscoff, France.

15 ⁵ Université de Perpignan Via Domitia, CNRS, CEFREM, Perpignan, France.

16 ⁶ Sorbonne Université, CNRS, Laboratoire d'Océanographie Microbienne (LOMIC), Observatoire Océanologique
17 de Banyuls-sur-Mer, 66650 Banyuls-sur-Mer, France.

18 ⁷ Université de Toulouse, CNES, CNRS, IRD, LEGOS, Toulouse, France.

19 ⁸ Météo-France, CNRS, Université de Toulouse, CNRM, Toulouse, France.

20 ⁹ Sorbonne Université, CNRS, Institut de la Mer de Villefranche (IMEV), 06230 Villefranche-sur-Mer, France.

21 ¹⁰ Sorbonne Université, CNRS, IRD, MNHN, LOCEAN, 75005 Paris, France.

22
23 *Correspondence to:* Laurent Coppola (laurent.coppola@imev-mer.fr)

24 25 **Abstract**

26 The annual MOOSE-GE cruise series is the backbone of the MOOSE regional ocean observing system providing a
27 unique dataset to observe and understand large-scale physical, biogeochemical and biological processes in the
28 northwestern Mediterranean basin, a key region that is responding to climate change faster than many other parts of
29 the world. These cruises address major scientific challenges, such as monitoring the variability and impact of deep
30 and intermediate convection, which plays a crucial role in deep-water ventilation, coastal–open ocean exchanges,
31 and the evolution of phytoplankton production in this highly dynamic system. They also allow the assessment of
32 climate change effects on ocean physics, marine biodiversity, biological resources, and seawater chemistry, including
33 oxygen, nutrients, and dissolved carbon. Sustained observations are required to track rapid trends such as increasing
34 temperature and salinity in intermediate and deep waters, declining oxygen concentrations, nutrients and carbonate
35 system inter-annual variabilities, expected increased stratification of the water column and variations in heat and salt
36 contents. These long-term datasets are indispensable both for climate model validation and process studies, as well
37 as for assessing the environmental status of the Mediterranean Sea. The data can be accessed at



38 <https://doi.org/10.18142/235> (Testor et al., 2010), <https://doi.org/10.17882/99825> (Bosse et al., 2024),
39 <https://doi.org/10.17882/44411> (Bosse et al., 2025), <https://doi.org/10.17882/45980> (Durrieu de Madron et al., 2024),
40 <https://doi.org/10.17882/43749> (Coppola et al., 2025), <https://doi.org/10.17882/99865> (Dimier et al., 2024).

41 **1 Introduction**

42 With around 160 million people living along its coasts, the Mediterranean Sea is under intense human pressure,
43 combining extremely high tourism density with very intense maritime activity (30% of global traffic). At the same
44 time, it is considered a global climate change hotspot (Giorgi 2006, Cramer et al., 2018; MedECC, 2020; IPCC,
45 2022), with significant impacts on its mean temperature, likely leading to intensified heatwaves, droughts, and heavy
46 precipitation events. The Mediterranean can be regarded as a natural laboratory for studying processes found in the
47 global ocean (deep convection, thermohaline circulation, etc.), but reacting more rapidly to climate shifts due to its
48 smaller volume. With a deep-water renewal time of only a few decades, compared to several centuries in the global
49 ocean, physical and chemical changes can be observed within a human lifetime (Schroeder et al., 2016). This
50 thermohaline circulation is closely linked to deep convection, whose intensity is projected to decline sharply in the
51 coming decades, or even to disappear (Somot et al., 2006; Parras-Berrocal et al., 2022). In addition, the saline outflow
52 from the Mediterranean through the Strait of Gibraltar is known to influence the North Atlantic Meridional
53 Overturning Circulation (Ivanovic et al., 2014), with direct impacts on water masses properties and associated
54 circulation. Thus, the Mediterranean is a semi-enclosed sea where circulation changes can directly influence the
55 global ocean.

56

57 In this context, the Northern Gyre is a key component of the cyclonic circulation system of the Northwestern
58 Mediterranean Sea (encompassing the Ligurian Sea and the Gulf of Lion) and driven by the combined effects
59 of wind forcing, buoyancy fluxes, and basin-scale circulation. It plays a central role in regulating water mass
60 transformation, deep convection and ventilation, controlling the redistribution of heat, salt, oxygen and
61 nutrients, and thereby strongly influencing biogeochemical cycles and ecosystem dynamics in the region
62 (Millot, 1999; Send et al., 1999; Houpert et al., 2016). As a result of these pressures, warming and salinification
63 of deep and intermediate waters have been observed in recent years (Schroeder et al., 2016, 2017; Houpert et al.,
64 2016; Margirier et al., 2020), with major impacts on decreasing dissolved oxygen content (Coppola et al., 2018),
65 nutrient concentrations (Belgacem et al., 2021), and carbonate chemistry (Wimart-Rousseau et al., 2023). In terms
66 of primary production, the Mediterranean Sea is an oligotrophic system with regions of intermittent blooms
67 (D'Ortenzio & d'Alcala, 2009; Mayot et al., 2017), for which the biological response to climate change and
68 anthropogenic pressures (e.g., variability of the nutrient inputs) remains unclear. Moreover, studies have highlighted
69 the significant role of continental inputs via the atmosphere and rivers, strongly impacted by human activity, on



70 biogeochemical cycles from the coast to offshore regions (Cossarini et al., 2015; Pasqueron de Fommervault et al.,
71 2015; Moon et al., 2016).

72

73 All these aspects call for a strong scientific basis to observe, understand, and model the marine environment. The
74 anticipated impacts of climate change and human activity in the Mediterranean fully justify maintaining a holistic,
75 multidisciplinary observation effort by coastal countries, with the aim of establishing a long-term European strategy
76 for Mediterranean observation. In this context, a French observing system, MOOSE (Mediterranean Ocean
77 Observing System for the Environment), was established in 2010 as a regional integrated observing network covering
78 the Northwestern Mediterranean, in the frame of MISTRALS program (Mediterranean Integrated Studies at
79 Regional And Local Scales) led by CNRS-led for 10 years and designed to build an integrated, multidisciplinary
80 understanding of the Mediterranean basin under global change, combining systematic observations, targeted field
81 campaigns, and modelling, and to support scenario-oriented knowledge (impacts on environments and societies).
82 MISTRALS relied heavily on sustained observing systems, and MOOSE is explicitly described as providing a “Long
83 Observation Period (LOP)” for several MISTRALS core components (HyMeX, MERMeX, ChArMEx), i.e., the
84 long-term backbone that complements shorter “intensive” campaigns (Drobinski, P., et al. 2014; MerMex group
85 2011; Sempéré et al., 2018). Thanks to the support of CNRS-INSU and the French Research Infrastructure ILICO
86 (CNRS, IFREMER), the network aims to observe and quantify long-term environmental anomalies, to characterize
87 seasonal and interannual variability, as well as the impact of extreme events on physical and biogeochemical
88 processes and marine biodiversity (Coppola et al., 2019; Cocquempot et al. 2021). MOOSE relies on a combination
89 of sites at sea and on land, monitored by ships, mooring lines and autonomous platforms to cover the wide range of
90 temporal and spatial scales. This mutli-platform approach is needed to understand the processes affecting the water
91 column (from the surface to the deep sea), the interactions between coastal and offshore zones, and between the
92 ocean, atmosphere, and rivers. The system is structured around four thematic work packages: WP1 (Mesoscale
93 circulation of the Northern Gyre), WP2 (Biogeochemical cycles and acidification), WP3 (Biodiversity and biological
94 resources), and WP4 (Continental and atmospheric inputs). The network has mainly focused on the continuous
95 collection of Essential Ocean Variables (EOVs), Essential Climate Variables (ECVs) and associated Essential
96 Biodiversity Variables (EBVs) and reliable descriptors, relying on techniques and procedures endorsed by different
97 scientific communities to ensure observational homogeneity across sites, promote shared analyses, and establish
98 common sampling and analysis protocols (best practices). The backbone of MOOSE network, contributing to WP1,
99 WP2, and WP3, are the annual “MOOSE Grande-Echelle” (MOOSE-GE) cruises, which provide a yearly basin-scale
100 overview in summer of the Northwestern Mediterranean Sea from surface to bottom, delivering essential variables
101 from physics to biogeochemistry and biodiversity.



102 Beyond its intrinsic regional value, MOOSE is fully complementary to other major Mediterranean observing systems
103 such as SOCIB in the Balearic Sea and POSEIDON in the Aegean and Ionian Seas, together forming a coherent
104 basin-scale observational framework (Tintoré et al., 2019; Mourre et al., 2023). While POSEIDON primarily
105 documents the formation and early transformation of intermediate and deep waters in the Eastern Mediterranean
106 (Kassis et al., 2012) and SOCIB focuses on high-resolution monitoring of exchanges and mesoscale-submesoscale
107 dynamics in key western transition zones such as the Ibiza Channel (Tintoré et al., 2013), MOOSE occupies a distinct
108 and downstream position in the Mediterranean thermohaline circulation. Its originality lies in its ability to monitor
109 the long-term evolution of intermediate and deep waters after their transit across the basin, and to directly observe
110 deep convection, dense water formation, and ventilation processes in the Northwestern region (including the Gulf of
111 Lion and the Ligurian Sea), the most dynamic region of the Mediterranean Sea (Testor et al., 2018). MOOSE thus
112 provides an integrated view of how variability originating in the Eastern Mediterranean propagates westward and
113 ultimately impacts deep water properties, oxygenation, biogeochemical cycles, and ecosystems. In this sense,
114 MOOSE complements SOCIB's process-oriented, high-frequency observations and POSEIDON's upstream
115 monitoring by offering a sustained, basin-integrating perspective, essential for closing the loop between water mass
116 formation, transformation, and long-term storage in the Mediterranean Sea.

117 **2 The cruise strategy**

118 The annual MOOSE-GE cruise series, initiated in 2010, has been an essential component of the MOOSE program
119 from its establishment. This large-scale network of stations aims to map the Northwestern Mediterranean Sea over
120 an area of 300,000 km² between the French southern coast, Menorca and Sardinia/Corsica. From 2010 to 2024, 60
121 to 130 stations were sampled each year for two weeks to one month between May and September, depending on the
122 size of the research vessel allocated by the French Oceanographic Fleet Research Infrastructure (French Ministry of
123 Research and Education, Table 1). This network makes it possible each year to sample the entire Northern Gyre in
124 order to monitor water mass properties (physical and biogeochemical) and their impact on the distribution of plankton
125 species. It also provides an annual reference state for the same EOVs acquired by autonomous platforms (Argo floats,
126 gliders) and the monthly monitoring stations at three sites: DYFAMED, ANTARES, MOLA (Figure 1).

127

128 The data collected during this cruise directly support the development of Good Environmental Status (GES)
129 indicators, in particular for Descriptor D1 (Biodiversity - Pelagic habitats) and Descriptor D5 (Eutrophication) of the
130 Marine Strategy Framework Directive (MSFD). The spatial coverage, resources deployed onboard, and hosting
131 capacities of the research vessels used during the MOOSE-GE cruise enabled the implementation of the
132 MEGASCOPE monitoring protocol. These data contribute to the assessment of GES indicators and Environmental
133 Objectives (EOs) for Descriptor D1 Biodiversity (marine mammals and turtles, seabirds) and Descriptor D10 (Marine



134 litter). Data are also essential for the development and validation of numerical models (e.g., SYMPHONIE) as well
135 as long-term climate models (CNRM, S. Somot) in the Mediterranean.

136

137 These repeated cruises allow the critical yearly maintenance of two moorings from EMSO European Research
138 Infrastructure Consortium (EMSO ERIC) (EMSO-LION and EMSO-DYFAMED), as well as two coastal moorings
139 integrated in MOOSE (PLANIER and LACAZE-DUTHIERS). Maintaining these systems requires substantial
140 operations (1–3 days of ship time per mooring) conducted in close collaboration among the laboratories involved in
141 the MOOSE network and EMSO-France (e.g., inter-calibration of mooring sensors with reference shipborne
142 measurements). Transits between mooring sites are used to perform hydrological sections across the study area (Gulf
143 of Lion, Balearic Islands, Ligurian Sea, Corsica/Sardinia). These hydrographic stations serve two purposes: 1)
144 calibrating moorings and autonomous platforms sensors deployed under MOOSE and EMSO-France, and 2)
145 providing a large-scale “snapshot” of the study region with additional analysis performed from water samples and
146 plankton nets (nutrients, dissolved inorganic carbon, phytoplankton pigments, zooplankton nets). The quasi-synoptic
147 completion of this network (in less than one month) provides an annual large-scale mapping of the distribution of
148 water masses and their hydrological, chemical, and biological properties.

149

150 In more detail, the MOOSE-GE cruises consist of four main activities (divided in two legs of 11 and 12 days):

- 151 1. Hydrographic stations (Conductivity, Temperature, Depth (CTD) with Niskin bottles): a CTD probe
152 equipped with temperature, salinity, dissolved oxygen, fluorescence, currentmeters (lowered-ADCP), and
153 an Underwater Vision Profiler (UVP) with 21 Niskin bottles are deployed to profile from surface to bottom.
154 Since 2017, 120-130 stations have been sampled each year, according to three categories:
 - 155 - Classical stations: water samples for nutrients and chlorophyll-a only.
 - 156 - Reference stations: one per day, including “classical” variables plus dissolved oxygen, salinity,
157 pigments, and carbonate chemistry on two meridional reference transects.
 - 158 - Biological stations: collection of zooplankton organisms (nets and Niskins). Around 15 stations include
159 zooplankton tows (three hauls each: two from 0-200 m and one from 0-500 m).
- 160 2. Mooring maintenance of LACAZE-DUTHIERS and PLANIER, as well as EMSO-France moorings
161 DYFAMED and LION.
- 162 3. Deployment and recovery of autonomous platforms such as Argo profiling floats and underwater gliders.
- 163 4. Student training, involving MSc and PhD students from the Oceanography program in Paris (Sorbonne
164 University, École Polytechnique).

165

166 With an average of 20-30 km spacing between stations, the MOOSE-GE network (Figure 1) does not resolve properly
167 mesoscale eddies in the region characterized by a small deformation radius of about 10km (Beuvier et al., 2012;



168 Escudier, et al., 2016), but it has still been able to opportunistically sample properties of small-scale deep water
169 eddies due to an extensive spatial coverage (Bosse et al., 2016, 2017). The distance between stations is however
170 reduced near the continental slope in order to resolve the permanent frontal circulation of the Northern Current and
171 the Western Corsica Current. At the basin scale (~400 km), this resolution provides thorough information on the
172 properties of key water masses (AW, LIW/WIW, WMDW), with about 15 stations per cross-basin transect. The
173 network was designed to capture the large-scale flow centered on the deep convection zone off the Gulf of Lion
174 (Testor, et al., 2018), and allows the monitoring of the dense water cascading from the shelf (Durrieu de Madron, et
175 al., 2013). Stations located on the continental slope are more closely spaced (depending on bathymetry), allowing
176 fine resolution of steep frontal gradients, which are stronger there than offshore or nearshore. The annual MOOSE-
177 GE monitoring cruise thus provides a unique basin-scale spatial coverage along the main circulation pathways, which
178 can be used to describe interannual variability of water mass properties (T, S, O₂) in relation to the dynamics of the
179 Northern Gyre, i.e., the system formed by the Northern Current and its recirculations (Northern Balearic Current and
180 Western Corsica Current).

181

182 MOOSE-GE also provides a unique opportunity to train MSc students (OACOS, Sorbonne University) as well as
183 many interns and PhD students in hands-on oceanographic fieldwork during a proper research cruise involving multi-
184 disciplinary experts of the region. Finally, because MOOSE-GE cruises follow the requirements of the SNO
185 framework, they ensure rapid dissemination of station data (from physics to biology) through CORIOLIS Global
186 Data Assembly Center (real-time) and SISMER, the French Research Vessel's database (delayed mode). Over the
187 years, they have become a recognized example of a repeated European-scale cruise, serving as a demonstrator for
188 both national projects (e.g., RIOMAR, FUTURE-OBS) and European initiatives involving several ERICs (e.g.,
189 Horizon EUROSEA, EA-RISE, and currently GEORGE).

190

191 To keep this important observational effort in a sustainable framework and in order to reduce the environmental
192 footprint of the ship, certain aspects of the sampling strategy (e.g. reduced transit speed, duration of the cruise,
193 optimisation of the stations) are being adapted without compromising the main scientific objectives. For example, a
194 transit speed of 8 knots between stations has been adopted since 2024 in order to reduce CO₂ emissions and
195 significantly reduce fuel consumption (respectively from 420 to 333 TCO₂ equivalent and from 110 to 87 T of
196 gazole). This adjustment has not significantly affected the proposed station network, which theoretically decreased
197 from 130 to 110 stations. In addition, MOOSE-GE's approach is being adapted to new techniques considering the
198 first results of the biodiversity sampling performed since 2017.

199

200 Since 2014, biodiversity monitoring has been based on sampling 15 biological stations, which were randomly
201 scattered across the basin in the various marine biological ecosystems (coastal vs offshore, oligotrophic vs



202 mesotrophic). After 10 years, this strategy has not allowed for detection of interannual trends, mainly due to (i) the
203 varying seasonal timing of MOOSE-GE cruises, and (ii) the dispersed geographical coverage, which prevents linking
204 observations to specific hydrographic structures. The recent analysis of the 2017-2019 cruises (spanning May to
205 September) highlighted this difficulty in interpreting biological data collected via imaging and genomics at variable
206 periods (Lescot et al., submitted to *Frontiers in Marine Science*). In 2024/2025, it has been decided that biodiversity
207 monitoring will focus on the two major north-south transects: Nice–Calvi (10 stations) and Marseille–Minorca (15
208 stations). This new strategy therefore not only doubles the number of biological stations (25 stations), but also allows
209 repeated sampling along well-characterized hydrographic gradients and provide day-night (nycthemeral) monitoring
210 of planktonic species across distinct water masses with different properties (e.g., temperature/salinity, nutrients). This
211 will enable the detection of a more precise biological signal over time and vertical space. Data exploitation will thus
212 be possible: (1) at the interannual scale, if the cruise periods are consistent across years; (2) through process studies
213 along the two transects, if cruise periods differ; or (3) following anomalous years (e.g., intense marine heatwaves).
214 The plankton net sampling strategy has been also revised, using one bongo nets to 200 m depth with 20 μm and 200
215 μm meshes, combining imaging (zooplankton) and genomic analyses (microbial and mesozooplankton diversity).

216

217 Until 2024, MOOSE-GE cruises had mainly focused on the offshore domain, and observations at interfaces (WP4)
218 lacked more spatially resolved and repeated monitoring of the Gulf of Lion’s shelf. Extension of the cruise network
219 to the Gulf of Lion shelf with 12 coastal stations has been adopted since 2024 for monitoring the Rhône river inputs
220 and their impacts on the biogeochemical properties of the water column (without increasing ship time, but by
221 optimizing the number of stations). This transect makes it possible to compare offshore signals driven by global
222 changes with coastal signals influenced by direct anthropogenic forcing. It also provides essential biogeochemical
223 measurements on the shelf, particularly to monitor the impact of Rhône inputs on carbonate chemistry (e.g., pH,
224 alkalinity) and to validate specific regional numerical model (e.g., SYMPHONIE ECO3M-S). High-frequency
225 monitoring of riverine inputs remains a central objective of the national coastal network such as COAST-HF and
226 SOMLIT (ILICO-RI), and it is therefore crucial to integrate this land-sea continuum observation within the MOOSE
227 network using the same strategy applied to offshore stations.

228 **3 Methods**

229 The MOOSE program (CNRS-INSU) has initially focused on ensuring the sustained acquisition of EOVs required
230 to meet the objectives of the different WPs, while also providing the basis for marine environmental descriptors,
231 particularly those related to eutrophication and biodiversity. To achieve this, MOOSE has relied on community-
232 endorsed techniques and procedures, with particular attention to: 1) ensuring their homogeneous application across
233 all sites and partners, 2) promoting shared analytical efforts, and 3) preparing common protocols for sampling and



234 analyses. MOOSE also relies on National Analytical Services (CNRS-INSU) that apply strict quality control
235 procedures (e.g., SAPIGH for pigments - Dimier et al., 2024, SNAPCO₂ for carbonate system parameters - Metzl et
236 al 2024). Data validation within MOOSE is carried out first by the scientists responsible for sites and/or platforms,
237 who comply with internationally recognized analytical protocols (standards, intercalibration exercises, comparison
238 with long-term climate series), and subsequently by the national data centers (SISMER, CORIOLIS), which perform
239 systematic checks before archiving (identification of outliers, doubtful values, etc.). This process allows each dataset
240 to be assigned a quality code (WOCE code in most cases).

241

242 **3.1 CTD rosette**

243 The number of CTD casts ranged from 57 to 137 (Table 1) from which seawater samples have been collected for
244 different physical, chemical and biological variables analysis (Table 2). All CTD profiles were performed from
245 surface to near bottom using an altimeter (5-10m above the seafloor) and Niskin bottles collected samples at standard
246 depths from surface (5m) to the deepest depth (max. 2850m). Once per day, water samples at three levels (surface,
247 salinity maximum of intermediate waters near 350m, bottom) were taken for salinity analysis. The samples were then
248 analyzed on board using a Guildline Autosol Salinometer. An offset from OSIL standard water varied from -0.005
249 to 0.005 depending on the laboratory temperature.

250

251 CTD system used for all MOOSE-GE cruises was a Seabird SBE9plus + CTD from Villefranche marine station
252 connected to a SBE11 deck unit, configured with a 12-position SBE32 pylon (from Villefranche or Marseille
253 laboratory) from 2010 to 2015 and a 24-position SBE32 pylon (from DT-INSU, Brest) since 2016 with 12 L Niskin
254 bottles (all years). The position of three Niskin bottles was occupied by the L-ADCP system and the UVP5 (sn002)
255 was mounted outside for the 12-bottle rosette and inside for the 24-bottle rosette. The CTD system was equipped
256 with two sensors for temperature and conductivity (SBE3 and SBE4) in order to improve the final data quality, one
257 oxygen sensor (SBE43) with a second since 2016 (JFE RINKO III), a fluorometer (Chlsea), and an altimeter. For
258 each cruise, sensors had been recently calibrated from the manufacturer (Seabird) and sensors have been rotated
259 every year, but the general system configuration remained exactly the same (except during some damages where).

260

261 Temperature, salinity, oxygen and pressure data were post-processed using Seabird's processing routines following
262 GO-SHIP's recommendations described in McTaggart et al. (2010) and in Uchida et al. (2010). MATLAB and more
263 recently PYTHON routines were used for the final quality assessment and control of Temperature, Salinity and
264 Oxygen data. Spikes were removed and adjusted 1-dbar bin-average profiles were archived on SISMER data server
265 (Testor et al., 2010: MOOSE-GE cruise series, <https://doi.org/10.18142/235>). To adjust the conductivity and oxygen
266 sensors installed on the CTD rosette, salinity and oxygen data were compared with reference bottles samples analyzed



267 with the salinometer and Winkler method, respectively. The different adjustments minimizing residuals (slope
268 coefficient on conductivity for SBE4; an iterative optimization adjusting three coefficients - SOC, VoffSet, E - for
269 SBE43) were carefully performed during the CTD profiles post-processing. This standard procedure ensures an
270 overall accuracy within the expected range for temperature (0.001°C), salinity (0.002 g/kg) and oxygen (+/- 2
271 µmol/kg).

272

273 **3.2 L-ADCP and S-ADCP measurements**

274 The shipboard Acoustic Doppler Current Profilers (S-ADCP) used during MOOSE-GE cruises depends on the year
275 and the ship (RDI's OS 150kHz (range 21-300m, dz=8m) for 2012, 2014, 2015 on RV Suroit, and 2013 on RV
276 Tethys; OS 150 and OS 38kHz (range 21-1200m, dz=24m) since 2016 on RV Thalassa, L'Atalante or Pourquoi Pas
277 ? (Bosse et al., 2024). MOOSE-GE cruises: lowered and ship ADCP data. SEANOE.
278 <https://doi.org/10.17882/99825>). The S-ADCP data averaged over a 2-min period were concatenated and processed
279 using Cascade V7.2 processing software (Kermabon et al., 2018) to compute horizontal ocean current velocities with
280 a spatial resolution of 2 km, corrected for navigation and ship attitude parameters, and filtered according to various
281 quality criteria (i.e., thresholds on vertical velocity error, vertical shear, correlation, minimum percentage of valid
282 ensembles, Kermabon et al., 2018). Bathymetry (Etopo 1 with 1 arc-minute resolution) was incorporated in the
283 processing to account for bottom detection. The profile data for the meridional and zonal components of the current
284 for the two S-ADCPs were combined to obtain a complete profile between 21 and 1200 m depth with maximum
285 resolution in the surface layer.

286 In addition to the S-ADCP measurements, current data have also been collected between the surface and the bottom
287 using a dual-head lowered acoustic Doppler current profiler (L-ADCP) system since 2012. Two 300kHz RDI
288 Workhorse ADCP current meter attached to the CTD-rosette were deployed in master/slave mode, one looking up
289 and one down. Data have been processed using the LDEO software (A.M. Thurnherr, "How to process LADCP data
290 with the LDEO Software (Versions IX.7-IX.10)", Internal report march 2014). External qualified data (CTD, S-
291 ADCP, GPS) are used to process L-ADCP data. S-ADCP data with a temporal resolution of two minutes for station
292 profiles were used to constraint the L-lowered ADCP data from the upper part of the water column (between the
293 surface and 1200 m deep).

294

295 **3.3 Underwater Vision Profiler (UVP)**

296 The Underwater Vision Profiler (UVP) was designed to measure the vertical distribution of macroscopic particles
297 larger than 100 µm and zooplankton larger than 1mm (Picheral et al., 2010). Its lower detection limit is set by optical
298 resolution, while the upper limit depends on the volume of water illuminated in each frame. The fifth-generation



299 UVP (UVP5) is a compact instrument (30 kg in air) that has been deployed as a stand-alone system with an
300 independent power supply on CTD-rosette package during the MOOSE-GE cruises (Rainer et al., 2022). It records
301 images at up to 6 Hz during the downcast of a CTD profile. The UVP5 therefore takes 5–25 pictures of the water
302 column, depending on the depth layers considered (1-5m). Image acquisition and analysis occur in real time with
303 direct return on-board when interfaced with a CTD. The particles in each image are counted and sized immediately,
304 and the data are stored in the instrument. Data were analyzed with the zooprocess software directly on-board with a
305 first quality control to only select timing corresponding to the profile. Data were afterward transferred to EcoPart
306 (<https://ecopart.obs-vlfr.fr/>) for final calculation of particle abundance and biovolume, while images were uploaded
307 to EcoTaxa (Picheral et al 2017; Irisson et al., 2022).

308

309 **3.4 Dissolved oxygen**

310 Dissolved oxygen measurements were obtained with a Seabird SBE43 sensor, calibrated against Winkler titrations
311 carried out on board. Water samples were collected once per day from CTD-rosette casts equipped with Niskin
312 bottles, spanning the water column from the surface to just above the seafloor. Winkler measurements were
313 performed using potentiometric detection of the equivalence point with a Metrohm 888 Titrando titrator between
314 2010 and 2018. Since 2019, a new system called “EndPoint” based a monochromatic wavelength spectrophotometer
315 to drive the titration dynamics and determine the final endpoint (Williams et al. 1982) was used, thereby increasing
316 the reproducibility of the measurements. The accuracy of the measurement was controlled with a KIO₃ standard
317 solution, prepared with dried potassium iodate dissolved in ultrapure water. The exact concentration of the homemade
318 KIO₃ standard was determined by titrating it against a potassium iodate standard solution of 0.0100N (WAKO).
319 SBE43 sensor calibration coefficients were refined for the entire cruise using the least-squares adjustment method
320 described in Coppola et al. (2018) and used in the CTD data post-processing method.

321

322 **3.5 Nutrients, chlorophyll-a and ammonium**

323 Samples for dissolved inorganic nutrients were collected from Niskin bottles in 20 mL polyethylene (HPDE) bottles
324 and filled with 100 µl of HgCl₂ solution (6 g/L) and stored onboard before being analyzed in the laboratory. They
325 were analyzed by a standard colorimetric method on a segmented flow analyzer (autoanalyzer Seal AA3 HR)
326 following Aminot and K erouel (2007). The limits of quantification are 0.03 µM for nitrite, 0.05 µM for nitrate, 0.03
327 µM for phosphate and 0.05 µM for silicate with a precision of 3%. Nutrient standardisation and data quality were
328 assured through successful and continuous participation in international intercalibration exercises. During the cruise,
329 measurements were further verified with the use of OSIL (OceanScientific International Ltd) marine nutrient
330 standards (ISO9001 accredited).



331 Chlorophyll-a concentrations were determined from discrete water samples collected in the water column.
332 Pigments were extracted in methanol and quantified onboard by fluorimetry following the protocol described
333 by Raimbault et al. (2004). The limit of quantification for chlorophyll a was $0.05 \mu\text{g L}^{-1}$, and the analytical
334 precision was estimated at 15%.
335 Ammonium concentrations were measured on board by fluorimetry following the method of Holmes et al. (1999).
336 The limit of quantification (LQ) was $0.02 \mu\text{M}$, and the analytical precision was estimated at 3%.

337 **3.6 Discrete CO₂ measurements (DIC, TA, pH)**

338 Samples for DIC and TA were collected into acid-washed 500 cm³ borosilicate glass bottles and poisoned with 200
339 mm³ of a half saturated HgCl₂ solution (final concentration of ca. 20 mg L^{-1}), following the recommendation of
340 Dickson et al. (2007). Samples were stored in the dark at 4°C pending analysis. Measurements of DIC and TA were
341 performed simultaneously on the same sample by potentiometric acid titration using a closed-cell following the
342 methods described by Edmond (1970) and Dickson and Goyet (1994). Analyses were performed at the National
343 facility for the analysis of carbonate system parameters (SNAPO-CO₂, Metzl et al., 2024) between 3 months and one
344 year after the end of the cruise. The average accuracy of AT and CT analysis (estimated from repeated measurements
345 of Certified Reference Material provided by Prof. Dickson's laboratory from the Scripps Institution of Oceanography,
346 San Diego) was between 2 and $4 \mu\text{mol.kg}^{-1}$ for the different MOOSE-GE cruises.

347
348 Since 2019, pHT (total pH) measurements were performed directly on board. Samples for pH measurements were
349 collected in cylindrical optical glass vials and analyses were performed manually using purified m-Cresol Purple
350 (mCP - provided by Prof. Byrne, University of Southern Florida) following the spectrophotometric protocol (at 25°C)
351 described by Clayton and Byrne (1993). pH is reported on the total scale at the temperature of measurement in the
352 lab (close to 25°C) using the equation by Liu et al. (2011). The reproducibility of measurements was estimated to be
353 ± 0.001 by measuring replicates from the same Niskin bottle. The accuracy was determined to range within ± 0.005
354 by analysing replicates of TRIS solution (provided by Prof. Dickson, Scripps Institution of Oceanography, San Diego
355 or by the Laboratoire National de Métrologie - LNE, Paris).

356

357 **3.7 Dissolved Organic Carbon (DOC)**

358 Since 2016, DOC sampling has been performed during the annual MOOSE-GE cruises along the two north–south
359 transects, Nice–Calvi and Marseille–Minorca (about 350 samples per year and 700 duplicate analyses). Samples are
360 collected into precombusted glass tubes and acidified with orthophosphoric acid (H₃PO₄) and analyzed in the



361 laboratory by high temperature catalytic oxidation (HTCO) on a Shimadzu TOCV analyzer. Typical analytical
362 precision is ± 0.1 - 0.5 (SD) or 0.2 - 1% (CV).

363

364 **3.8 Phytoplankton pigments**

365 Phytoplankton pigments have been collected once per day since the start of the MOOSE cruises. The seawater was
366 collected by Niskin from surface (5m) to 150m and filtered through GF/F filters (Φ 25 mm, $0.7 \mu\text{m}$ pore size,
367 Whatmann, Germany) for HPLC (High Performance Liquid Chromatography) measurements, were preconditioned
368 under constant mild vacuum (not exceeding 0.5 bar), flash freeze in liquid nitrogen and successively stored at -80
369 $^{\circ}\text{C}$. The filtration volumes varied from 1000 to 3520 mL. The samples have been analysed by a CNRS-INSU national
370 service (SAPIGH) based in Villefranche/Mer laboratory. The service uses HPLC method to measure chlorophylls
371 and carotenoids in the marine environment (Dimier et al., 2024). It enables the separation and quantification of >25
372 different pigments that provide information on the biomass, composition and photo-physiological status of
373 phytoplankton communities.

374 **3.9 Biodiversity data**

375 The monitoring of biological variables using quantitative imaging instruments relies on multiple devices (UVP,
376 Zooscan, FlowCam, and now Planktoscope), following the procedures established by the Quantitative Imaging
377 Platform of Villefranche-sur-Mer (an EMBRC-labeled platform) on several nets tows (20, 64, 200 and 500 μm).
378 Samples from the nets were fixed with either formalin (4% final concentration, buffered with borax) or acidic Lugol
379 solution (for the $20\mu\text{m}$ net tows) and analyzed on land. Only the Planktoscope ($20\mu\text{m}$ net) samples were imaged alive
380 on-board. Samples were analyzed with protocols as described in the following protocols: Perruchon et al. (2025) for
381 the Planktoscope, Jalabert et al (2025a) for the Zooscan, Jalabert et al (2025b) for the Flowcam. Description and
382 units of the final images data and associated metadata are described for the different instruments in Picheral &
383 Mériquet (2025).

384

385 For environmental DNA (eDNA) monitoring, samples from plankton nets are filtered through $10 \mu\text{m}$ pore-size filters
386 and then frozen in liquid nitrogen. For seawater collection with Niskin bottles, three depths are sampled (surface,
387 chlorophyll maximum, and deep > 2000 m). After pre-filtration at $200 \mu\text{m}$, these samples are sequentially filtered
388 onto $3 \mu\text{m}$ and $0.2 \mu\text{m}$ filters to target planktonic species (metabarcoding and metagenomics). Filters are then stored
389 in liquid nitrogen until data acquisition. DNA extraction and library preparation protocols follow standards
390 established in international initiatives (e.g., Tara Oceans, EMO-BON) and are available here:
391 <https://www.protocols.io/private/7007EF8B81BE11F093E50A58A9FEAC02>. DNA extraction protocol is detailed
392 on the online protocol repository [protocols.io: dx.doi.org/10.17504/protocols.io.kxygxy5xdl8j/v1](https://doi.org/10.17504/protocols.io.kxygxy5xdl8j/v1). About $1 \mu\text{g}$ of



393 pooled amplicons were sent to Fasteris-GeneSupport (www.fasteris.com, Plan-les- Ouates, Switzerland) for high-
394 throughput sequencing on a 2×250 bp MiSeq Illumina. Amplification and library construction is detailed on
395 protocols.io: dx.doi.org/10.17504/protocols.io.bzucp6sw.

396

397 **3.10 Deep moorings and sediment traps**

398 The PLANIER and LACAZE-DUTHIERS moorings, at the eastern and western ends of the Gulf of Lion, are
399 equipped with PPS3 sediment trap (Technicap) and Aquadopp current meters at 500 and 1000 metres deep. The
400 LION and DYFAMED moorings are equipped with SBE37 (CT sensors), SBE37-ODO (oxygen sensors), SBE56
401 (temperature sensors), and Aquadopp current meters, deployed from 100 m below the surface down to 2300 m. In
402 addition, LION includes a PPS3 sediment trap at 2300 m, which is designed to collect particles originating from the
403 settling of surface material, the resuspension of local sediment and lateral inputs from the Gulf of Lion shelf and
404 canyons (Stabholz et al., 2013; Durrieu de Madron et al. 2017). DYFAMED, on the other hand, is equipped with two
405 PPS5 sediment traps at 200 m and 1000 m, which collect marine snow as well as biogenic and lithogenic particles
406 derived from biomass blooms and atmospheric inputs (Miquel et al., 2011; Heimburger et al., 2013).

407 The CTD profiles and discrete bottle samples collected during the cruises provide the primary calibration and quality-
408 control reference for the mooring-based observations. Moorings are serviced annually to recover one-year datasets
409 and sediment-trap samples (preserved in 5% formaldehyde), to limit biofouling, and to ensure metrological
410 consistency across successive deployments. During each servicing, mooring sensors are cross-calibrated against the
411 shipborne CTD-rosette (with recently calibrated sensors) using dedicated comparison casts performed at 2-3 target
412 depths (typically near-surface, 300-400 m, and ~ 1000 m). Sensors are held at each level for ~ 30 minutes, enabling
413 the detection and correction of deployment-related sensor drift and offsets, as well as inter-sensor consistency checks
414 along the mooring line. After recovery, moored time series undergo delayed-mode processing including pressure-
415 dependent corrections, despiking, temporal coherence checks, and the identification/removal of biofouling-related
416 artefacts, with particular attention to low-frequency drifts affecting conductivity and dissolved oxygen
417 measurements. After adjustment of T, S, and O_2 data, these observations allow the detection of basin-scale variability
418 with high accuracy (0.001 °C, 0.005 g/kg, Houpert et al., 2016; ± 2 $\mu\text{mol/kg}$, Coppola et al., 2018). This
419 measurement protocol has been documented in a best practice report for Eulerian measurements described by
420 Coppola et al. (2016) and published by Pearlman et al. (2019).

421 The processing of Aquadopp current meter records involves several steps to produce clean, validated hourly time
422 series for pressure, temperature, and horizontal current speed and direction. First, the raw data are offloaded from the
423 instrument and converted to scientific units using manufacturer calibration routines. Quality control procedures such
424 as spike removal, gross error filters, and flagging of suspect records are applied to exclude outliers and faulty



425 measurements. For vertical speed, the instrument's movements on the mooring line, identified from pressure records,
426 are subtracted from the measured vertical velocity to correct for mooring motion.

427 **3.11 Argo floats deployment**

428 The recurrent deployment of T-S-O₂ profiling floats and BGC floats is carried out during the annual MOOSE-GE
429 cruises (deployment and/or recovery). Since 2012, more than 42 Argo floats have been deployed in the western
430 Mediterranean basin, of which 6 remain active in 2025 (4 ARVOR TS, 1 PROVOR-DO and 1 PROVOR BGC). The
431 Argo float sampling strategy is tailored to the western basin, with profiles from 0–2000 m every 5 days (0-1000 m
432 for BGC floats) and a parking depth of 1000 m, resulting in horizontal spacing of 1-50 km between successive profiles
433 from the same float. Some floats are specifically dedicated to biogeochemistry and operate on daily cycles at 1000m.
434 Mediterranean profiling floats typically have a lifetime from 2 to 5 years, providing a description of basin-scale
435 evolution that complements the monitoring carried out during MOOSE cruises, glider transects, and fixed moorings,
436 while quantifying the temporal and spatial variability of these variables at the scales accessible to this technology.
437 During the MOOSE-GE campaigns, some Argo floats reaching the end of the battery have been recovered every year
438 (around 2-4 floats per year).

439 **3.12 Sensors calibration and data correction**

440 Sensor calibration and correction procedures are fundamental to the MOOSE observing system, as they
441 underpin climate studies based on long-term monitoring and provide a robust reference for ocean model
442 evaluation. In particular, the ability to detect and quantify subtle changes in water mass properties is essential
443 for documenting climate-driven trends, especially in deep and intermediate waters where long-term variations
444 in temperature, salinity and dissolved oxygen are small but climatically significant (Somot et al. 2018; Coppola
445 et al. 2018). Within MOOSE, rigorous calibration and data correction procedures are therefore implemented to
446 ensure the long-term consistency and traceability of physical and biogeochemical observations acquired by
447 CTD-rosette systems and autonomous mooring sensors. All CTD measurements collected during the monthly
448 cruises and the annual MOOSE-GE campaigns rely on shipborne rosette systems equipped with high-accuracy
449 temperature, conductivity and pressure sensors, operated following international best practices (GOOS/OBPS)
450 and calibrated every year by the manufacturers. Pre- and post-cruise laboratory calibrations are complemented
451 at sea by systematic comparisons with discrete water samples: salinity is calibrated against IAPSO Standard
452 Seawater using Guildline Autosal analyses, while dissolved oxygen sensors are calibrated using Winkler
453 titrations. These reference measurements are used to derive sensor-specific correction coefficients, which are
454 applied uniformly to the full CTD profiles. During the annual MOOSE-GE campaigns, dedicated CTD stations
455 are additionally performed in the immediate vicinity of deep moorings (e.g. DYFAMED, LION, Planier and



456 Lacaze-Duthiers canyons) to cross-calibrate autonomous sensors (see section 3.10). All corrections are
457 documented and applied in delayed-mode processing, ensuring internal consistency between Eulerian
458 (moorings, ship stations) and Lagrangian platforms (gliders, Argo floats), for which the ship-based CTD
459 observations serve as regional calibration references. The resulting quality-controlled datasets constitute the
460 backbone of the MOOSE long-term time series and provide a robust and traceable basis for detecting climate
461 signals, evaluating numerical models and quantifying long-term changes in Mediterranean water mass
462 properties.

463 **4 Data availability**

464 The flow of data produced in real time or in delayed mode is considerable, and its management represents a true
465 challenge for the observing system in terms of quality control (QC), formatting, archiving, and integration into
466 databases. As the MOOSE program is embedded in a national context (with research infrastructures linked to DATA
467 TERRA and the marine hub ODATIS), a European context (ERICs), and an international framework of observation
468 efforts (EUROGOOS and GOOS), its data component naturally follows the international standards recommended at
469 these levels (e.g., EMODnet). This ensures greater interoperability between databases, broad dissemination, and
470 consequently better scientific exploitation of these observations. Interoperability is crucial both at the organizational
471 level within MOOSE (integration of multi-site data) and at the European and international levels (recognition and
472 increased collaboration potential). Existing protocols (quality control procedures, data formats, interoperability
473 standards), already established through consensus in international and European projects, have therefore been
474 adopted by the MOOSE network.

475 Data presented in this study are available from SISMER <https://doi.org/10.18142/235> (Testor et al., 2010) and from
476 SEANOE: <https://doi.org/10.17882/99825> (Bosse et al., 2024), <https://doi.org/10.17882/44411> (Bosse et al., 2025),
477 <https://doi.org/10.17882/45980> (Durrieu de Madron et al., 2024), <https://doi.org/10.17882/43749> (Coppola et al.,
478 2025), <https://doi.org/10.17882/99865> (Dimier et al., 2024).

479 For data processing and archiving of the cruises, MOOSE relies on the effort of national data centers and the ODATIS
480 data hub of the DATA TERRA RI. In particular:

- 481 - CTD casts profiles are transmitted in near-real time directly to the CORIOLIS Global Data Assembly Center
482 (GDAC) for operational oceanography. It includes temperature, salinity, and oxygen profiles collected and
483 processed onboard. CTD data is transmitted within a short delay (< 24h, but usually <1h) after SBE
484 automated processing, then qualified and stored following Coriolis real-time standards. This operational
485 task has been automated by a cruise server developed during the MOOSE-GE cruises and installed on the



486 ship's network allowing for a centralisation, and easy access of all stations data sets. Once the cruise is
487 finished, the server's data are imported online to be archived (<https://www.medship.org/doku.php>).

488 - CTD casts profiles, bottles and mooring data are transmitted in delayed-mode (DM) after sample analyses
489 and S and O₂ sensors adjustment (with seawater sampling and cross-validation for mooring sensors).
490 Processing can take several months, and in some cases more than a year for Niskin samples. Once QC and
491 validation are complete, data is transferred to the SISMER center for cruise-based data, and to Coriolis for
492 mooring data (OceanSites/EMSO format).

493 - Additional datasets, such as L-ADCP, chlorophyll pigments (HPLC) are also available via SEANOE
494 landing pages. This provides several advantages: (1) access to detailed metadata, (2) rapid DOI assignment,
495 (3) fast availability of data in multiple formats, with the possibility of later updates, and (4) automatic
496 generation of a list of publications using or referencing the dataset. This type of repository is also valuable
497 for revised compilations of legacy datasets. SEANOE provides access to data not archived by SISMER
498 despite being collected during cruises (non-standard SISMER data format).

499
500 For imagery data (UVP5, Zooscan), processing (taxonomic sorting) and storage are carried out through the web
501 application EcoTaxa (Picheral, 2017), which subsequently enables data dissemination to aggregators such as
502 EMODnet and OBIS. Particle counts, concentrations and obtained identifications (if available) from UVP profiles
503 are also directly downloadable from EcoPart. Processing efficiency is partly ensured through machine learning: users
504 can train models based on prior identifications in the database to suggest labels for newly uploaded images. By
505 combining deep-learning feature extractors, a fast-training classifier, and sufficient flexibility to build task-specific
506 models, EcoTaxa achieves classification performances comparable to state-of-the-art deep learning networks, while
507 remaining usable within minutes by taxonomists with no background in computer science. For environmental
508 genomics, raw data are deposited in the European Nucleotide Archive (ENA) and subsequently integrated into the
509 "Ocean Barcode Atlas" server (OBA; Vernet et al., 2021), together with associated environmental (physical and
510 chemical) metadata. In coordination with national initiatives (FUTURE-OBS) and European ones (EMO-BON), a
511 sequencing data processing pipeline (meta-barcoding) has been developed to ensure both the reproducibility of
512 analyses for future sample processing and the interoperability of different biodiversity data types (sequences and
513 images).

514 **5 Results and discussion**

515 Although the concept of the MOOSE program is based on an integrated vision of all available data in the NW
516 Mediterranean basin, the MOOSE- GE cruises have highlighted some major results:



- 517 - Increase in the heat and salt content of the LIW (data obtained from the EMSO-LION and EMSO-
518 DYFAMED moorings, later validated and corrected with cruise data) and propagation of LIW changes
519 throughout the basin (Margirier et al., 2020).
- 520 - Detailed monitoring of the vertical structure of the deep waters (not captured by Argo floats profiling at
521 2000 dbar maximum) which documented at the scale of the oceanic basin the intense event of dense waters
522 cascading from the Gulf of Lion's shelf in 2012 (Durrieu de Madron et al., 2013), the impact of shelf and
523 open-ocean convection on particles distribution (Durrieu de Madron et al., 2017), the subsurface mesoscale
524 eddy field (Bosse et al., 2016) and its coupling with biogeochemistry (Bosse et al., 2017), as well as the
525 recent warming of deep waters and vertical structure during years of reduced deep convection intensity
526 (Bosse et al., 2024).
- 527 - Development of a prediction algorithm for carbonate and nutrient variables based on using predictions from
528 a neural network (CANYON-MED), trained with cruise data from 1986 to 2018, including MOOSE-GE
529 (Fourrier et al., 2020 and 2022).
- 530 - Detection of trends in nutrients with an increase in deep waters (Belgacem et al., 2021, Fourrier et al. 2022).
- 531 - Detection of an increase in inorganic carbon and a decrease in pH in surface, intermediate and deep waters
532 in the Ligurian sea based on MOOSE-GE data and other MOOSE time series (Coppola et al. 2020; Metzl
533 et al. 2024).
- 534 - Three distinct zooplankton groups were identified in 2017 based on integrated 0-200 m values of
535 environmental variables: the first with stations mainly located in the Ligurian Sea, and the other two in the
536 northern and southern parts of the Provençal basin, highlighting a marked north-south gradient (PhD thesis
537 of G. Feliu, 2020)
- 538 - The increased frequency of the MOOSE-GE cruises in collaboration with the HyMeX, MerMEX and
539 DeWeX programmes during the year 2012-2013 allowed to assess the seasonal cycle of the NW
540 Mediterranean deep water mass characteristics from August 2012 to June 2013 and, for the first time to our
541 knowledge, to estimate with only in-situ observations the WMDW Formation rate of that record-breaking
542 convective year (Waldman et al. 2016, Testor et al. 2018).

543

544 **5.1 Physical variables**

545 The deep-water temperature in the NW Mediterranean Sea increasing of about 0.3 °C has already been observed
546 since the 1950s (Bethoux et al., 1990; Krahnemann, 1998), and projections to 2100 predict a strong rise in surface



547 temperatures (Darmaraki et al. 2019, Soto-Navarro et al. 2020), which could notably disrupt the reproductive cycles
548 of many marine species (Lejeusne, 2010). This evolution is closely linked to the phenomenon of winter convection
549 induced by cold, dry winds (Mistral and Tramontane) channeled by the surrounding mountain ranges of the Gulf of
550 Lion (Estounel et al., 2016). Convection ventilates intermediate and deep waters, modifying their properties. The
551 induced vertical mixing can reach great depths in the open-ocean off the Gulf of Lion, a zone preconditioned by
552 cyclonic ocean circulation. Episodes of mixing down to the seabed (2500 m) were observed in February during the
553 winters of 2009 to 2013 (Houpert et al., 2016). Since then, winter mixing has reached much shallower depths (300-
554 500 m on average, except in 2015 and 2018 when mixing was more active down to about 1500 m, Margirier et al.,
555 2020). Winter convection can be tracked by satellite using ocean colour imagery (Herrmann et al., 2017) prior to the
556 spring bloom, the largest in the Mediterranean, typically observed in April as the water column restratifies.

557 In this context, CTD profiles collected throughout the entire water column during the annual MOOSE-GE cruises
558 provide a valuable long-term monitoring of intermediate waters (mainly Levantine Intermediate Water, LIW) and
559 deep waters (Western Mediterranean Deep Water, WMDW). The compilation of historical MOOSE-GE datasets
560 highlights strong interannual variability, characterized by a rapid increase in temperature and salinity within both
561 LIW and WMDW (Fig. 2 & 3). These data reveal a marked interannual to decadal variability in deep ocean
562 convection (Testor et al., 2018; Somot et al., 2018, Margirier et al. 2020). Winters from 2010 to 2013 were
563 distinguished by bottom-reaching convection events (down to 2400 m), whereas since 2014 winter mixing has been
564 considerably weaker, largely due to weaker buoyancy losses induced by the atmospheric forcing and enhanced
565 stratification of the water column (Margirier et al., 2020, Josey and Schroeder 2023). As a consequence of weaker
566 mixing rate between the intermediate and deep layers over the recent years, and a strong advection of warmer and
567 saltier LIW flowing to the Western Mediterranean Sea at the Strait of Sicily (Schroeder et al., 2017), waters between
568 200 and 600 m have warmed significantly by about 0.5 °C within a decade and within the whole Northwestern basin.
569 This intermediate-depth warming is progressively transferred to deeper layers: since 2019, waters below 2000 m
570 have warmed continuously down to the seabed at a rate of about 0.002 °C yr⁻¹, driven by turbulent mixing that slowly
571 conveys heat from the LIW to the deep waters in the absence of deep convection.

572 **5.2 Biogeochemical variables**

573 The northwestern Mediterranean is a highly dynamic region due to the intense convection and ventilation processes
574 that occur in winter (Conan et al., 2018; Coppola et al., 2017). These processes lead to rapid changes in the content
575 of biogeochemical elements (gases, nutrients), with implications for phytoplankton production. The impact of
576 physical processes on bloom dynamics, through physical–biogeochemical coupling in the mixed layer and the
577 resulting vertical fluxes, remains poorly understood, and integrated observations can provide new insights.



578 The combined MOOSE-GE cruise data show that dissolved oxygen (DO) in LIW and WMDW is strongly modulated
579 by shifts in convection regimes. During the period of intense deep convection (2010-2013), enhanced ventilation led
580 to higher DO in both water masses, with LIW concentrations reaching about 190 $\mu\text{mol/kg}$ and 210 $\mu\text{mol/kg}$ in the
581 WMDW (Fig. 4). In contrast, during the subsequent weak-convection period (2014-2024), reduced vertical mixing
582 limited oxygen renewal in intermediate and deep layers while respiration and organic-matter remineralization
583 continued. The decline is particularly evident in the LIW, where the oxygen minimum layer progressively intensified
584 and expanded vertically in the absence of regular convective events (Coppola et al., 2018), with DO now reaching
585 $\sim 170 \mu\text{mol/kg}$. Deep waters also exhibit a marked decline over this period, with an DO decrease of approximately 1
586 $\mu\text{mol/kg/yr}$ and WMDW concentrations now around 190 $\mu\text{mol/kg}$ (Fig.4). Episodic convective winters partially
587 interrupted this decline by temporarily increasing DO, but these effects remained short-lived. Overall, the MOOSE-
588 GE observations indicate that the LIW and WMDW are now significantly less ventilated, with a clear and persistent
589 decline in DO that is particularly pronounced and in particular in the LIW (Fig. 4). This pattern is consistent with a
590 slowdown of deep convection under ongoing Mediterranean warming, which reduces episodic oxygen renewal while
591 oxygen consumption by respiration and remineralization continues. Although oxygen levels remain well above
592 hypoxic thresholds, the emerging LIW deoxygenation signal warrants close monitoring, as it could intensify if
593 regional warming and stratification strengthen further in the coming decades.

594 The annual and monthly MOOSE cruises have provided valuable insight into the seasonal variability of nutrient
595 concentrations throughout the water column. Winter vertical convection supplies surface layers with nutrients,
596 directly fueling primary production (Mayot et al., 2017). As a result of intense biological uptake, nutrient
597 concentrations in surface waters decrease rapidly during spring and remain low, sometimes close to detection limits,
598 from June to October. Despite strong interannual variability, this seasonal cycle is recurrently observed from year to
599 year. Beyond this seasonal signal, the multi-decadal perspective offered by the MOOSE-GE cruises has enabled
600 recent studies to address the long-term evolution of nutrient concentrations. The nutrient time series indicates a
601 sustained increase in nutrient concentrations in deep waters (below 2000 dbar) since 2010, particularly for nitrate
602 and silicate (from 8.5 to 9.2 $\mu\text{mol/L}$ and from 8.5 to 10 $\mu\text{mol/L}$, respectively; Fig. 5), with this long-term trend being
603 intermittently weakened during strongly convective years (e.g. 2011 and 2013). These trends are interpreted as the
604 combined result of modified deep-water formation rates, changes in ventilation, and enhanced remineralization
605 processes at depth (Fourrier et al., 2022). Since 2014, and again after 2018, MOOSE-GE observations reveal a rapid
606 increase in nitrate and silicate concentrations in deep waters (Fig. 5). This evolution is likely associated with a
607 slowdown of deep convection events, leading to reduced ventilation and the establishment of more homogeneous
608 deep-water masses. Under these conditions, remineralization products progressively accumulate at depth, resulting
609 in increasing nitrate and silicate inventories. In contrast, phosphate exhibits a weaker and, in some periods, opposite
610 trend, with a slight decrease in deep-water concentrations. This behavior likely reflects a decoupling between nitrogen



611 and phosphorus cycles, driven by differential remineralization rates and changes in water mass composition
612 associated with the formation and spreading of new Western Mediterranean Deep Water, with a possible contribution
613 from preferential phosphorus removal through particle-associated processes (Krom et al., 2004; Pasqueron et al.,
614 2015; Schroeder et al., 2016). The resulting increase in deep-water N:P ratios suggest a progressive strengthening of
615 phosphorus limitation in the north-western Mediterranean Sea and highlights the strong sensitivity of deep
616 biogeochemical reservoirs to changes in ventilation and overturning dynamics.

617 The MOOSE time-series observatories provide also a unique basis for assessing the evolution of the carbonate system
618 in the north-western Mediterranean Sea across seasonal to decadal time scales. High-quality measurements of total
619 alkalinity (TA) and dissolved inorganic carbon (DIC) collected during monthly cruises and annual MOOSE-GE
620 surveys reveal a pronounced seasonal cycle in surface waters, with winter maxima linked to vertical mixing and
621 summer minima associated with biological carbon uptake (Coppola et al., 2019; Wimart-Rousseau et al., 2023). It has
622 to be noticed that, for an unexplained reason, DIC and TA data collected during MOOSE-GE 2017 have an unusually
623 high amount of data that have been considered as doubtful during the quality-control procedures and the carbonate
624 data from this year should be considered with caution. In contrast, TA exhibits comparatively weak seasonal
625 variability, reflecting the dominant control of salinity and the limited influence of biological processes. At longer
626 time scales, MOOSE-GE observations over 2010-2024 indicate that TA increased slowly until 2017 before reaching
627 a relatively constant value in intermediate and deep waters (~ 2600 and ~ 2590 $\mu\text{mol/kg}$ for LIW and WMDW,
628 respectively; Fig. 6), while salinity increased steadily over the same period (by ~ 0.35 over 15 years in the LIW; Fig.
629 3). Although TA often covaries with salinity in open-ocean settings, TA trends in the Mediterranean Sea cannot be
630 inferred from salinity changes alone, as increases are also observed in salinity-normalized alkalinity (Metzl et al.,
631 2024). For DIC, the same trend has been observed : an increase of concentrations from 2010 to 2017 (up to 2355 and
632 2335 $\mu\text{mol/kg}$ for LIW and WMDW, respectively) and an apparent stabilization to constant values from 2018 to
633 2024 for both water masses (Fig.6). These trends are consistent with those reported by Wimart-Rousseau et al. (2023)
634 and are further supported by the multi-platform analysis and machine learning predictions of Fourier et al. (2022),
635 which demonstrates that DIC accumulation and pH decline (observed at DYFAMED from Yao et al., 2016; Merlivat
636 et al., 2018; Coppola et al., 2020; Wimart-Rousseau et al., 2023) are strongly modulated by intermittent deep
637 convection. Periods of intense mixing temporarily slow down acidification by ventilating intermediate and deep
638 layers and by injecting waters with higher pH into depth, whereas prolonged stratified periods favor the accumulation
639 of remineralized carbon and accelerate acidification in the absence of renewal. The observed increase in DIC,
640 combined with largely stable TA, reflects the uptake of anthropogenic CO_2 and the redistribution of carbon through
641 both physical and biological pumps, with intermediate waters playing a key role in carbon sequestration.



642 **5.3 Biodiversity variables**

643 The impacts of climate change and anthropogenic pressures in the Mediterranean are expected to cause major shifts
644 in biodiversity, as well as in the structure and functioning of marine ecosystems, which could ultimately degrade
645 resource quality and disrupt human uses such as fisheries. One objective of the MOOSE-GE cruises is to establish a
646 systematic monitoring of plankton communities from end to end (from viruses to zooplankton), including
647 prokaryotes, phytoplankton, micro- and mesozooplankton, in relation to environmental variables. This approach aims
648 to provide a comprehensive overview of biodiversity trends and, ultimately, their consequences on the
649 biogeochemical and trophic functioning of the pelagic ecosystem. More specifically, we focus on describing
650 biological diversity in a variable oceanographic context, using simple and standardized sampling procedures for all
651 diversity data collected during the cruises (annual and monthly). To this end, we rely on imaging methods for
652 zooplankton analyses, and also propose to integrate recently developed environmental genomics methods for the
653 microbial and mesozooplankton compartments (during annual cruises only). This new approach will provide access
654 to the specific and functional diversity of small organisms that play a central role in ocean biogeochemistry but are
655 difficult to detect with conventional methods. The combination of both approaches will allow us to monitor and
656 understand the evolution of plankton communities as a whole, and to detect new non-indigenous and newly
657 introduced species in relation to climate warming.

658 Zooplankton samples are collected using vertical net hauls (200 μm mesh, from 0 to 200 m) following international
659 standard protocols (Harris et al., 2000). Since 2014, MOOSE has processed these samples using imaging methods
660 (Zooscan, FlowCam, stereomicroscope), applying identical protocols across monthly stations and during the
661 MOOSE-GE cruises (Fig. 7). Imaging time series provide both quantitative data (abundance, size, biovolume) and
662 qualitative data (taxonomic groups, target groups, dry weight), which can be easily linked with physical, chemical,
663 and biological databases. These analyses enable mapping of zooplankton biomass and abundance distributions, as
664 well as taxonomic groups or even key species, and allow the study of spatial variations in relation to environmental
665 parameters. Recently, imaging and taxonomic data distinguished three zooplankton groups based on integrated 0-
666 200 m values: one group corresponding mainly to Ligurian Sea stations, and two others located in the northern and
667 southern parts of the Provençal basin, revealing a marked north–south gradient (Feliu thesis, 2020). Zooplankton
668 abundance and biomass in the Ligurian Sea and southern Provençal basin are relatively homogeneous, while the
669 largest variations are observed on the Gulf of Lion slope and in the central Provençal basin.

670 The integration of environmental genomics, as a complementary activity of the MOOSE network, was initiated in
671 2017 by the Roscoff, Marseille and Villefranche laboratories. It builds on the experience held with long term time
672 series obtained in the Mediterranean Sea and of genomic observatories at marine stations and *Tara* expeditions, and
673 follows international standards in the field (Santi et al., 2024). This new approach aims to: (1) describe the biological



674 diversity of plankton assemblages in an oceanographic context; (2) implement a simple, standardized sampling
675 procedure to be integrated into long-term monitoring; and (3) rapidly disseminate meaningful data to the community.
676 Samples are collected using plankton nets and Niskin bottles. The latter allow microbial diversity to be studied along
677 the water column through (1) metabarcoding analyses of plankton assemblages in two size fractions (0.2 to 3 μm for
678 bacteria/picoeukaryotes, and 3 to 200 μm for phyto/small zooplankton), and (2) metagenomic analyses to assess
679 prokaryotic functions. Net samples are used to describe the molecular diversity of phyto and zoo-plankton
680 components ($>20 \mu\text{m}$, $>200 \mu\text{m}$) and to quantify mesozooplankton through *in situ* automated imaging (UVP). During
681 each MOOSE-GE cruise, around 400 samples are collected for genomic analyses. Over the years 2017, 2018, and
682 2019 plankton community structure was primarily shaped by organism size and water column depth, with smaller
683 fractions (0.2-3 μm and 3-180 μm) in the surface and deep chlorophyll maximum layers showing the highest alpha
684 diversity. Larger fractions ($>64 \mu\text{m}$) were dominated by metazoans, particularly Arthropoda, while smaller size
685 classes were dominated by protists such as Syndiniales and Rhizaria. Seasonal shifts were detected in small size
686 fractions, especially for diatoms and dinoflagellates, while larger size fractions exhibited weaker temporal variability.
687 Physical clustering of stations revealed clear cross-shelf and basin-scale gradients, which aligned more with
688 community structure at fine taxonomic resolution (ASV level) for smaller fractions.

689 **5.4 Links to the modelling community**

690 MOOSE has maintained strong links with the SIROCCO Community Code, particularly for products derived from
691 the coupled SYMPHONIE ECO3M-S model (Marsaleix et al., 2008; Estournel et al., 2016). MOOSE network data
692 are highly valuable as they cover several north–south transects across the basin, an annual mesoscale grid, and high-
693 frequency fixed-point time series encompassing the full water column. These data have notably enabled the validation
694 and improvement of simulations of carbon production and export (Ulses et al., 2016; Kessouri et al., 2017), nutrient
695 cycles (Kessouri et al., 2018) dissolved O_2 content (Ulses et al., 2021), as well as the simulation of the annual and
696 seasonal budgets of dissolved inorganic carbon (DIC), during 2012-2013 (Ulses et al., 2023).

697

698 Looking ahead, simulation products developed and validated with MOOSE data, specifically aiming to: 1) provide
699 annual and seasonal simulations of the mixed layer depth, SST, nutrient, chlorophyll, O_2 and air-sea CO_2 fluxes, 2)
700 extract time series at geolocated points for temperature, salinity, O_2 , nutrients, alkalinity, pH, and DIC in intermediate
701 and deep waters, complementing *in situ* monthly observations and/or discontinuous datasets, 3) provide closed budget
702 for heat, salt, carbon, nitrogen, phosphorus and oxygen, and 4) propose, in collaboration with the SIROCCO
703 Community Code, value-added products such as annual heatwave indicators, including the spatial extent and the
704 depth of the water column affected by marine heatwaves.

705



706 In addition, MOOSE data are used as reference dataset for the development of ocean stand-alone and fully coupled
707 regional climate models in particular within the international Med-CORDEX initiative (Ruti et al. 2016) and the
708 national SiMED modelling group (<https://confluence-meteofrance.atlassian.net/wiki/spaces/SiMED/overview>).
709 More specifically, MOOSE datasets have served for model evaluation, calibration and selection as well as to create
710 model initial conditions or blended climate indices mixing in-situ data, satellite and models for studies dedicated to
711 the northwestern Mediterranean Sea. To cite some examples, MOOSE data (surface buoy, deep mooring, ARGO
712 floats, gliders) have been used to create model initial 3D state for studying the 2012-2013 case study (Estoumel et
713 al., 2016; Waldman et al. 2017), to evaluate the model air-sea interface at the LION buoy (Waldman et al. 2017),
714 deep water formation rate for the 2012-2013 year (Waldman et al. 2016), interannual variability of the yearly
715 maximum mixed layer depths and convective surfaces (Somot et al. 2018), water column stratification (Somot et al.
716 2018), trends in bottom water mass characteristics (Somot et al. 2018), thermohaline cell downward branch along
717 the bathymetry (Waldman et al. 2018). .

718

719 **5.5 The future of the MOOSE-GE cruises**

720 In order to improve efficiency and maximize the use of available research vessels, environmental fingerprints and
721 funding resources, MOOSE plans to optimize annual ship time by reducing the overall cruise duration while focusing
722 efforts on north–south transects (Nice-Calvi and Marseille-Minorca) and the Corsican/Sardinia areas, where the
723 signal of salinity is more intense (passage of the LIW) and pre-condition the convection event, to improve coverage
724 of coastal–open ocean exchanges and enhance observations of CO₂ systems and planktonic communities. In the
725 context of automated technologies (floats, gliders, moorings), regular cruises remain necessary for sensor
726 maintenance, data recovery and accuracy (e.g., seawater samples as reference data). Expanded deployment will
727 improve spatial and temporal coverage but comes with limits: 1) Argo floats drift with currents and the spatial
728 coverage is not guarantee, 2) sediment traps on moorings require annual maintenance to preserve and collect
729 biological samples sensing the degradation and mechanical issues (e.g. motor beneath the traps to rotate the sampling
730 bottles), 3) glider operations require manpower (2-3 months endurance, 0-1000 m depth only) and collect information
731 down to 1000m only with limited variables (T, S, O₂, Chla, CDOM, backscattering), 4) biological samples can only
732 be collected at sea (nets and seawater sampling).

733

734 In this context, MOOSE is involved since 2018 in the development of artificial intelligence tools (e.g., machine
735 learning method; Fourrier et al., 2020) based on the Argo community work for the global ocean (Sauzède et al., 2016;
736 Bittig et al., 2018). Indeed, CANYON-MED has been developed and trained from a huge dataset where MOOSE-
737 GE cruise data have been predominant. It was used to estimate nutrient and carbonate system trends from simple,
738 accurate variables at intermediate and deep waters where climate change impacts have been observed (Fourrier et al.,



739 2022). However, extreme events, recurrent in the Mediterranean yet unpredictable, require regular data acquisition,
740 especially during short-term duration events (e.g., marine heatwaves, coastal upwelling, ocean deep mixing,
741 cascading events, intense blooms). One of MOOSE's objectives is to characterize the marine environment during
742 such events and estimate their short-term (seasonal) basin-scale impacts. Consequently, regular training (5–10 years)
743 of these tools is needed to strengthen their capacity while maintaining data quality and require repeated cruises such
744 MOOSE-GE to cover a large basin scale area especially the Mediterranean Sea where resident time of water masses
745 and physical/biogeochemical processes are changing very fast.

746

747 To optimize the future of the cruises, OSSE (Observing System Simulation Experiment) approaches will be explored
748 to adapt ship time allocation, the number of stations along transects and the vertical resolution for bottle sampling.
749 The two main north–south transects in the NW basin (Nice–Calvi, Marseille–Minorca), as well as secondary sections
750 (e.g., Minorca-Sardinia-Corsica, gulf of Lion shelf), will be maintained because of their scientific importance (e.g.,
751 salinity propagation and its impact on mixing events, plankton community distribution, mesoscale circulation, river
752 inputs and cascading impacts...). Other options have also been considered, such as reducing vessel speed (down to
753 8 knots) to lower fuel consumption and CO₂ emissions, optimizing instrument deployment time through new
754 techniques (particularly for moorings), and carefully selecting sensors to minimize battery use, facilitate data
755 recovery, and reduce calibration costs. As shown in the pioneer work of Waldman et al. (2016), optimizing the
756 MOOSE-GE network will require to well define the list of the key scientific objectives we would like to address with
757 the future network configuration and the scientific questions that we accept to abandon with respect to the current
758 network and to an optimized one. Trade-off between the MOOSE-GE cost and scientific objectives will have to be
759 carefully selected and documented.

760 **6 Conclusion**

761 The MOOSE-GE cruise series constitutes a cornerstone of sustained, basin-scale observation in the northwestern
762 Mediterranean Sea, providing a unique, internally consistent record (2010-2024) of physical, biogeochemical and
763 biodiversity Essential Ocean Variables from the surface to the seafloor. In the Mediterranean context, this observing
764 effort is exceptional in scope and continuity: the annual repetition of a large, standardized cruise with a high number
765 of stations, the integration of multiple variables, research infrastructures synergy, measurement technologies and the
766 systematic inter-calibration with deep moorings and autonomous platforms have no equivalent in the basin.
767 Maintaining this capability is critical to resolve long-term trends and interannual variability across key processes
768 from deep convection and water-mass transformation to oxygenation, nutrient and carbon-cycle dynamics, and
769 ecosystem responses, especially as climate-driven impacts intensify. Such sustained basin-scale surveys should
770 therefore be regarded as a mandatory component of institutional and European observing strategies, requiring strong,



771 long-term support from oceanographic fleets and research infrastructures. Only with this level of commitment can
772 the community deliver robust, timely and quantitative scientific assessments and early-warning signals for the
773 Mediterranean Sea.

774

775 **Author contributions**

776 LC coordinates the MOOSE program and the annual MOOSE-GE cruises with PT and AB. TW, DL, ML, FC, FL,
777 FC, XDM, MPJ, PC participate actively in the cruise's preparation, analysis on board and data treatment. ER, CL,
778 ML, MG, PB, SK, JS and SN lead the instruments deployment, maintenance, samples collection and data analysis
779 and treatment. CU, CE and SS assist for model simulations and cruise scenarios.

780 **Competing interests**

781 No competing interests

782 **Acknowledgements**

783 The authors wish to pay tribute to the memory of Pascal Conan, who passed away on August 5, 2025. He made
784 insightful contributions and was unwaveringly dedicated to biogeochemical oceanography. We will miss him both
785 professionally and personally. The authors also wish to pay tribute to the memory of Francois Carlotti, a marine
786 biology researcher, who sadly passed away. His contributions and commitment will be deeply missed. We
787 acknowledge the sustained financial support from CNRS and the national research infrastructures ILICO and EMSO-
788 France, as well as the essential contribution of the French Oceanographic Fleet (FOF) for providing access to research
789 vessels. We also warmly thank all staff from the partner laboratories of the SNO MOOSE network for their
790 commitment at every stage of the program, from cruise preparation and field operations to sample processing,
791 analyses, and data quality control. Finally, we acknowledge the SISMER and Coriolis data-management teams, and
792 the support of the ODATIS data hub, whose efforts are critical to ensuring long-term stewardship, interoperability,
793 and open access to the MOOSE-GE datasets.

794 **Financial support**

795 The MOOSE program is supported by CNRS-INSU and by the French research infrastructures ILICO and EMSO-
796 France (French Ministry of Higher Education and Research). Additional support was provided by the FUTURE-OBS



797 project (Augmented Observatories for Coastal Socio-Ecosystems; ANR-22-POCE-0004), which funded part of the
798 genomic analyses, and by the RIOMAR project (Observing and Anticipating the Evolution of River-Dominated
799 Ocean Margins in the 21st Century; ANR-22-POCE-0006), which supported part of the biogeochemical analyses.

800

801

802

803

804

805

806

807

808

809

810

811

812

813

814

815

816



817 **Table 1: MOOSE-GE cruise ship, dates, duration and station numbers and depth levels performed each year**
 818 **from 2010 to 2024 (from the first to the last station, excluding the mobilisation/demobilisation days)**
 819

Period	Ship	Stations	Depth levels	Duration (days)
25 May 2010 - 29 June 2010	TETHYS II	55	12	34
28 May 2011 - 01 July 2011	TETHYS II	66	12	34
24 July 2012 - 08 Aug. 2012	SUROIT	89	12	15
11 June 2013 - 09 July 2013	TETHYS II	78	12	27
04 July 2014 - 22 July 2014	SUROIT	94	12	17
10 July 2015 - 27 July 2015	SUROIT	81	12	16
19 May 2016 - 09 June 2016	L'ATALANTE	84	21	20
31 Aug. 2017 - 23 Sept. 2017	L'ATALANTE	123	21	22
14 May 2018 - 06 June 2018	L'ATALANTE	121	21	22
08 June 2019 - 01 July 2019	THALASSA	118	21	23
COVID period	No ship available	NaN	NaN	NaN
09 June 2021 - 02 July 2021	THALASSA	135	21	22
07 Sept 2022 - 30 Sept. 2022	POURQUOI PAS	118	21	22
27 July 2023 - 18 Aug 2023	THALASSA	131	21	22
23 June 2024 - 16 July 2024	L'ATALANTE	113	21	22

820
 821
 822



823 **Table 2: Data acquired during the MOOSE-GE cruises with frequency and methodology**

824

Variables	Depth level	Frequency	Instruments/methods
T, S, O ₂ , fluorescence, PAR	Surface-bottom profile	All stations	Seabird 911, SBE3, SBE4, SBE43, Chelsea Aqua 3, WetLabs C-Star
Currents	Surface-bottom profile	All stations	L-ADCP RDI
Particles and zooplankton	Surface-bottom profile	All stations	UVP5 Hydroptic
Dissolved oxygen	21 depths	Once per day	Winkler
DIC-TA	21 depths	North-South sections	Potentiometry
pH (since 2019)	21 depths	North-South sections	Spectrophotometry
Nutrients	21 depths	All stations	Colorimetry
TChl-a, NH ₄	6 depths (surface-150m)	All stations	Fluorometry
Salinity	3 depths (surface, 350m, bottom)	Once per day	Guideline Autosal (electric conductivity)
Pigments	6 depths (surface-150m)	Once per day	HPLC (High-Performance Liquid Chromatography)
Phytoplankton and microbes	5 depths (surface, DCM, 350m, 1000m, 2000m)	North-South sections	Metabarcoding 18S rRNA gene
Phytoplankton	Nets 0-200m	North-South sections	Metabarcoding 18S rRNA gene, Planktoscope, Flowcam, MEB
Zooplankton	Nets 0-200m	North-South sections	Zooscan and Metabarcoding 18S rRNA gene

825
 826
 827
 828
 829
 830
 831



832
 833
 834
 835

Table 3: List of DOI for archived data in the framework of the MOOSE-GE cruises

Dataset	Period	Format	Archiving	DOI
CTD profiles	2010-2024	NetCDF, ODV	CORIOLIS (NRT), SISMER (DM), SeaDataNet	10.18142/235
Bottles sampling	2010-2024	NetCDF, ODV	SISMER, SeaDataNet	10.18142/235
L-ADCP, S-ADCP	2012-2021	NetCDF	SEANOE	10.17882/99825
Pigments	2013-2022	ASCII	SEANOE	10.17882/99865
UVP, Nets	2013-2025	TSV or ASCII	EcoPart / EcoTaxa (one project/year)	Ecopart project number : 15, 17, 18, 31, 55, 100, 149, 168, 483, 576, 783, 1041, 1254; Ecotaxa Projects: 30, 853, 2436, 5771, 6851, 7705, 7709, 10367, 14620, 10304, 13555, 13906 xxxx
Nets	2015-2025	TSV + images	EcoTaxa (one project/year/ instrument)	Project number: Flowcam : 825, 2278, 2481, 4961, 7589, 11300, 14546, Planktoscope : 6818, 13760, 13937, 17816, 2784, Zooscan : 14, 492, 493, 497, 828, 896, 3402, 4598, 6048, 7058, 7906, 11687, 15780, 19379
metaB sequences	2017-2019	fastQ	ENA/EBI	PRJEB76575
DYFAMED mooring	1988-2024	NetCDF	CORIOLIS/SEANOE	10.17882/43749
LION mooring	2007-2024	NetCDF	CORIOLIS/SEANOE	10.17882/44411



LACAZE mooring	1994-2024	NetCDF	CORIOLIS/SEANOE	10.17882/45980
PLANIER mooring	1994-2024	NetCDF	CORIOLIS/SEANOE	10.17882/45980

836

837

838

839

840

841

842

843

844

845

846

847

848

849

850

851

852

853

854

855

856

857

858

859

860

861

862

863

864

865

866



867
868
869
870
871
872
873
874
875
876
877
878
879
880
881
882
883
884
885
886
887
888
889
890
891
892
893
894
895

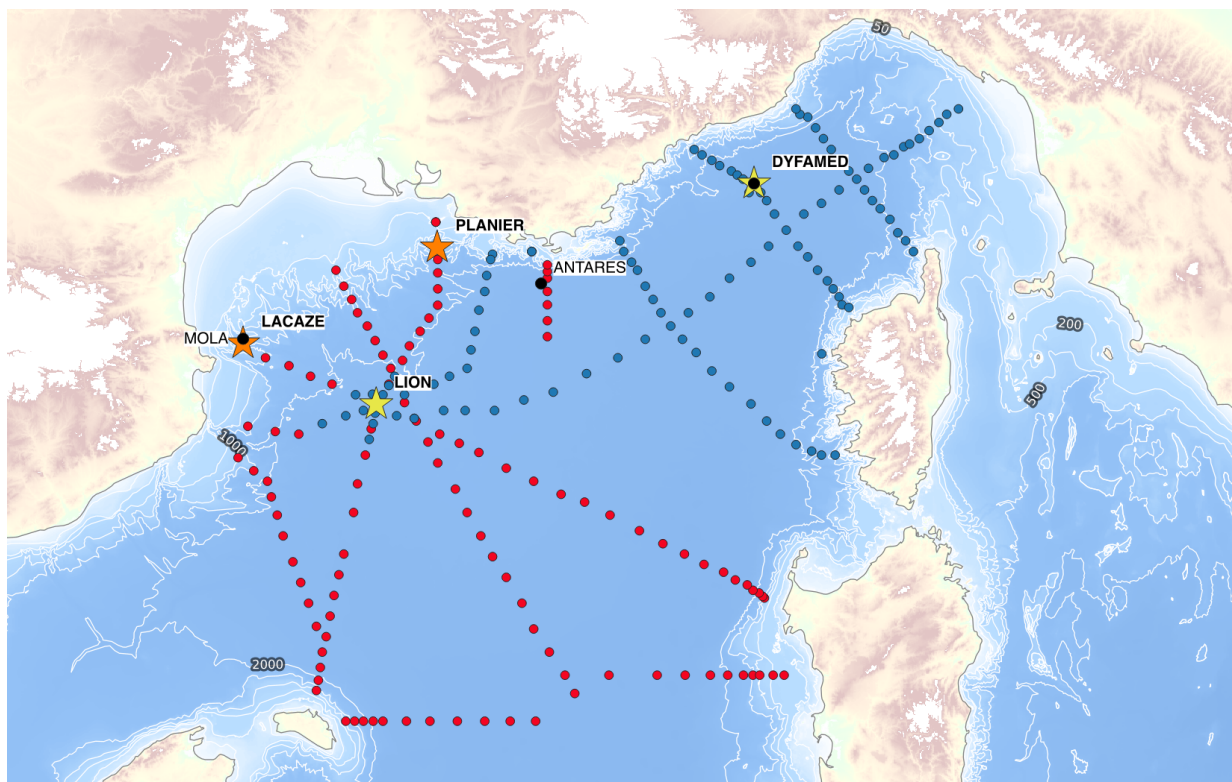
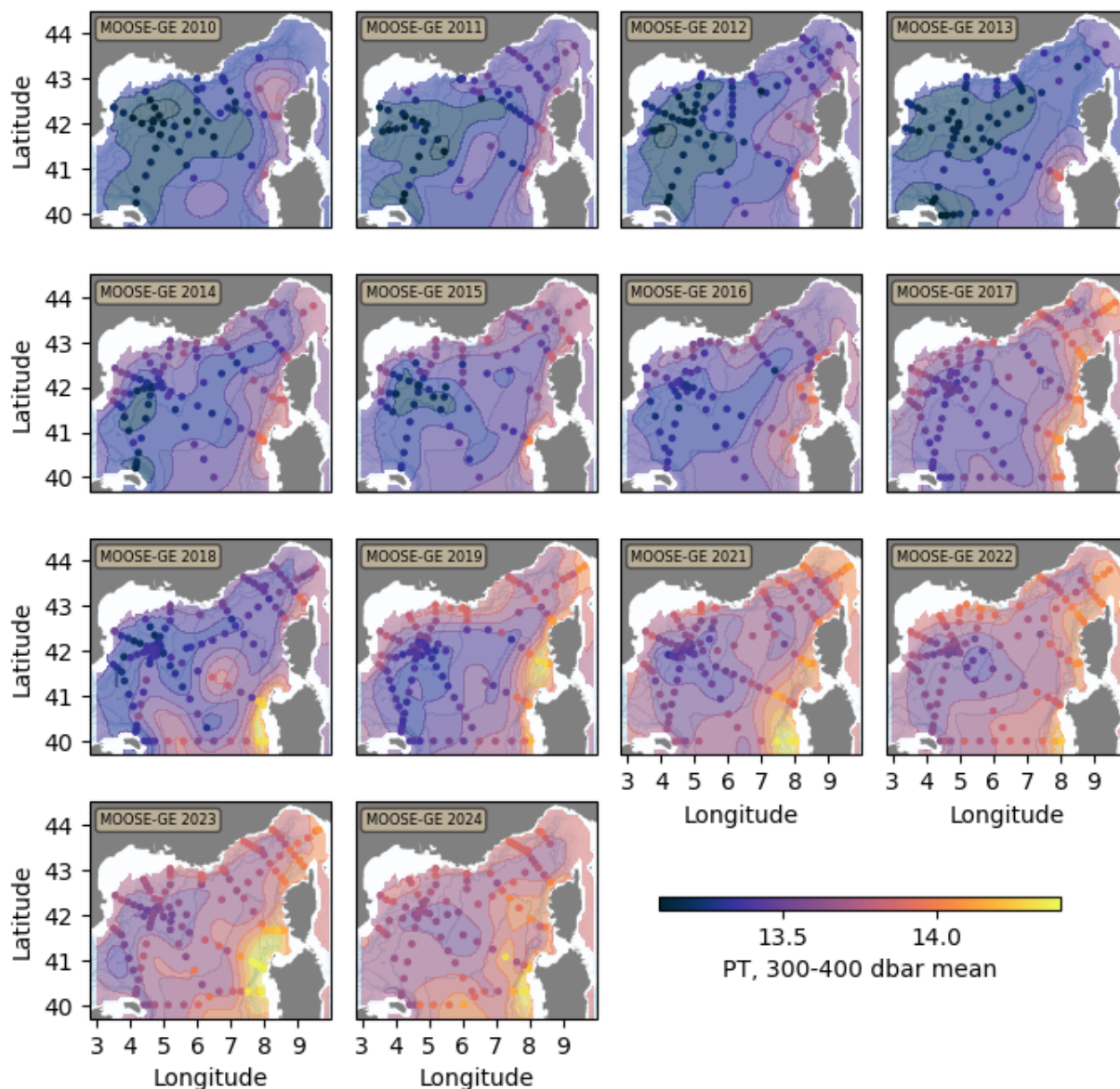


Figure 1: Map of the MOOSE-GE cruises showing LEG1 (blue dots) and LEG2 (red dots) stations. EMSO moorings (DYFAMED, LION) are shown as yellow stars, canyon moorings (Lacaze, Planier) as orange stars, and sites with monthly visits as black dots (Mola, Antares, Dyfamed).



896

897



898

899

900 **Figure 2: The station map illustrates each year the spatial distribution of potential temperature between 300**
901 **and 400 dbars in the northwestern Mediterranean basin from 2010 to 2024**

902

903



904
905
906
907
908
909
910
911
912
913
914
915
916
917
918
919
920
921
922
923
924
925
926
927
928
929
930
931
932
933
934
935
936

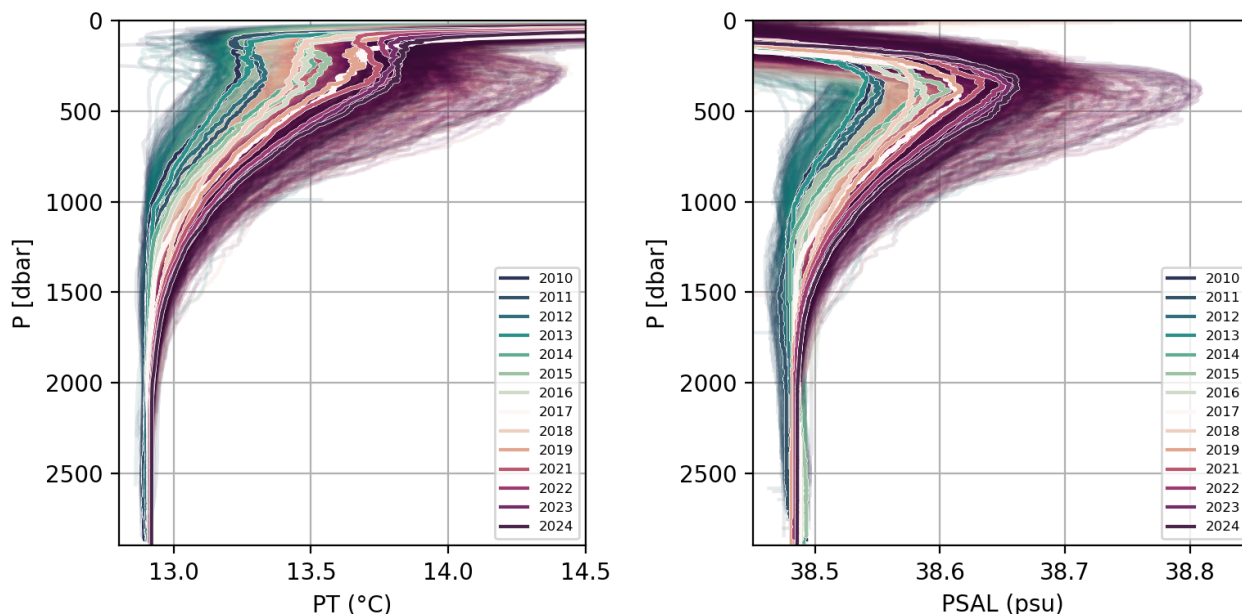


Figure 3: Potential temperature and practical salinity vertical profiles during the MOOSE-GE cruises from 2010 to 2024. The color represents the different years.



937
938
939
940
941
942
943
944
945
946
947
948
949
950
951
952
953
954
955
956
957
958
959
960
961
962
963
964
965
966
967
968
969
970

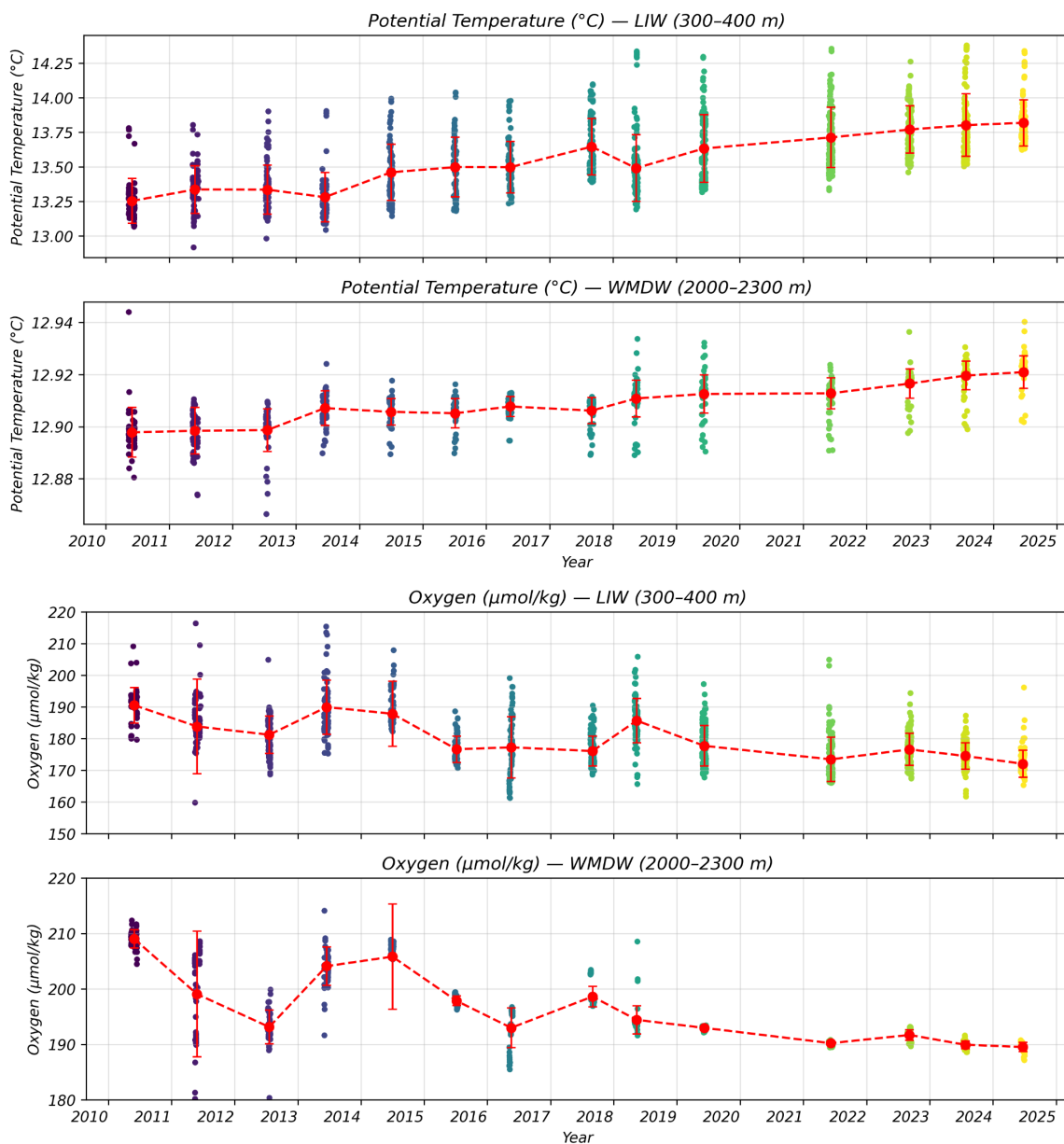


Figure 4: Time series of potential temperature (top panel) and dissolved oxygen (bottom panel) at LIW and WMDW core depth levels (300–400m and >2000m, respectively). The color represents the year and the red dots the average value for each year with the standard deviation.



971

972

973

974

975

976

977

978

979

980

981

982

983

984

985

986

987

988

989

990

991

992

993

994

995

996

997

998

999

1000

1001

1002

1003

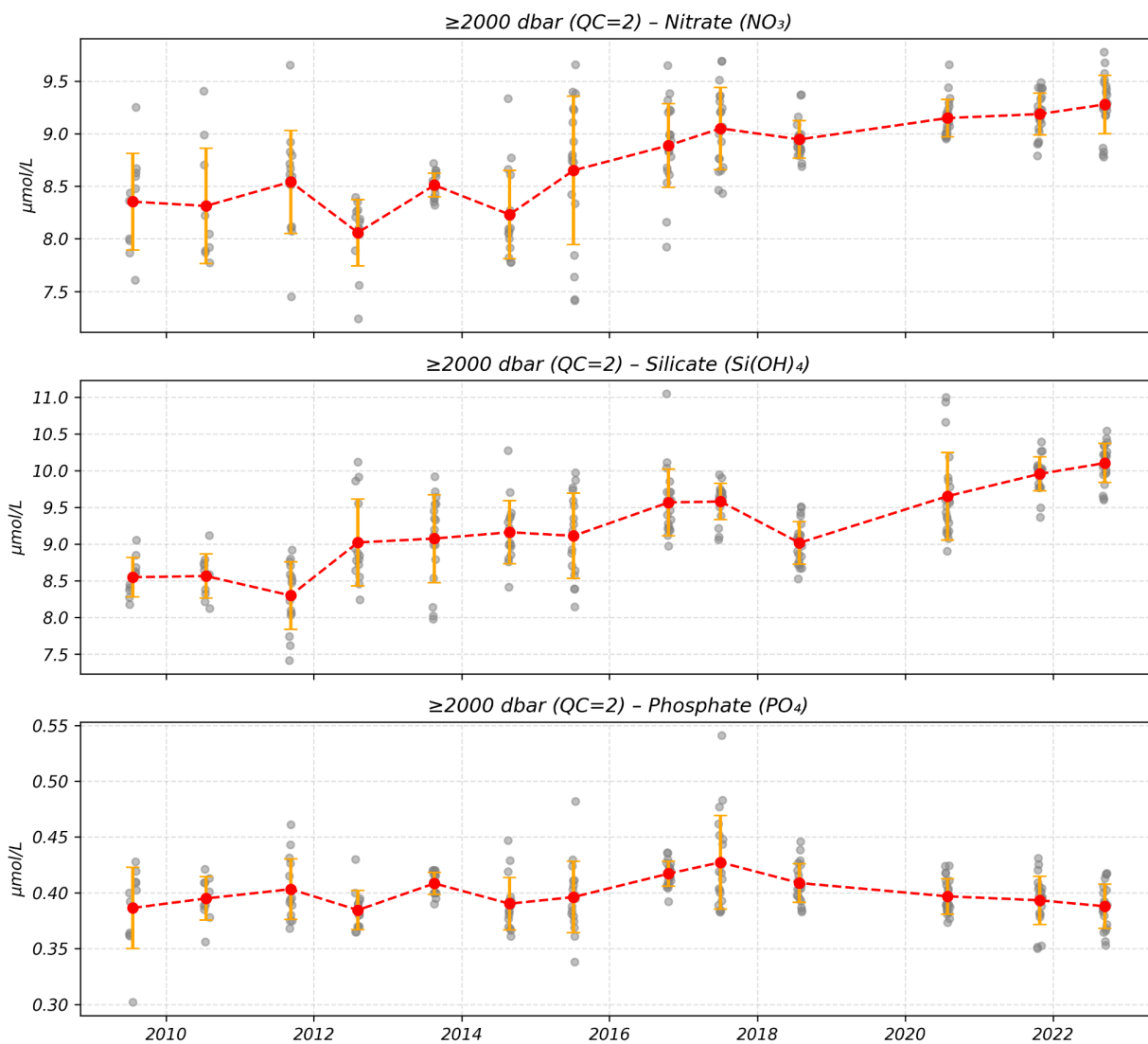


Figure 5: Evolution of nutrients concentrations (in $\mu\text{mol/L}$) in the deep waters ($> 2000\text{m}$) acquired during the MOOSE-GE cruises. The red dots represent the annual mean with the standard deviation



1004
1005
1006
1007
1008
1009
1010
1011
1012
1013
1014
1015
1016
1017
1018
1019
1020
1021
1022
1023
1024
1025
1026
1027
1028
1029
1030
1031
1032
1033
1034
1035
1036
1037

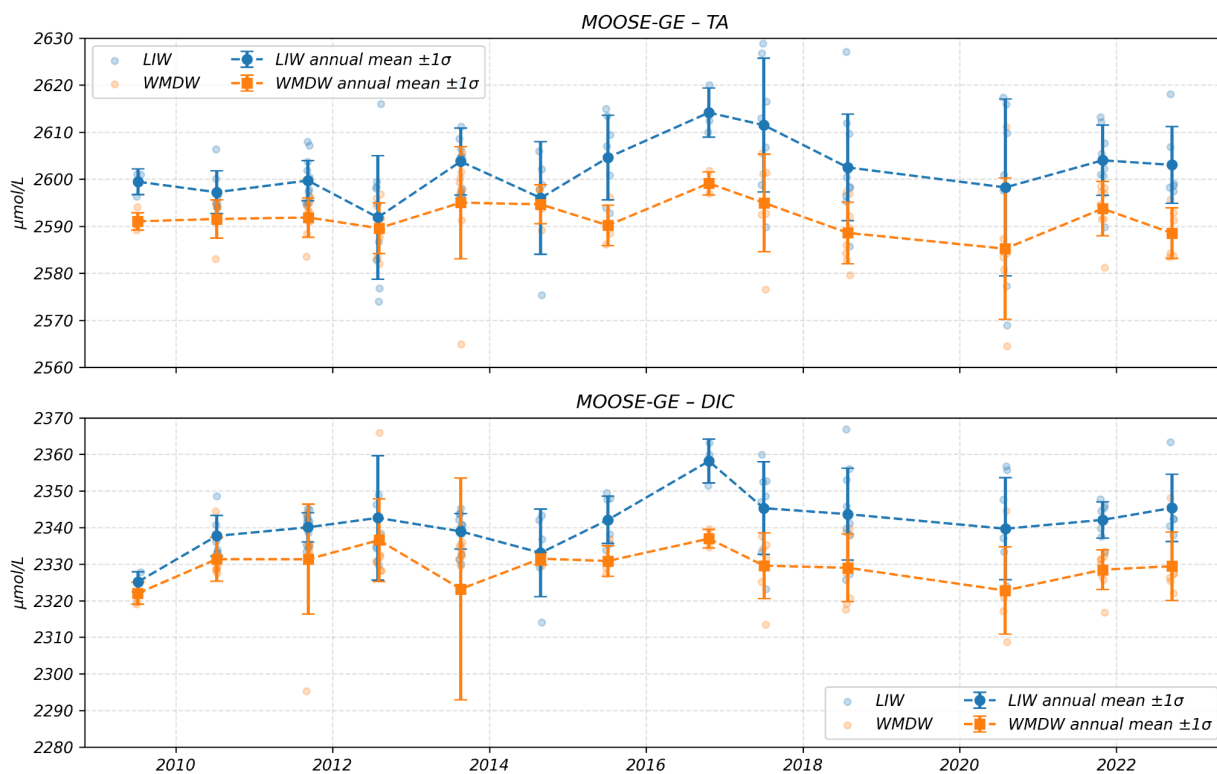


Figure 6: Evolution of TA and DIC concentrations (in $\mu\text{mol/L}$) in the intermediate waters (400-600m) in blue and in the deep waters (> 2000m) in orange acquired during the MOOSE-GE cruises. The dots represent the annual mean with the standard deviation



1038
1039
1040
1041
1042
1043
1044
1045
1046
1047
1048
1049
1050
1051
1052
1053
1054
1055
1056
1057
1058
1059
1060
1061
1062
1063
1064
1065
1066
1067
1068
1069
1070

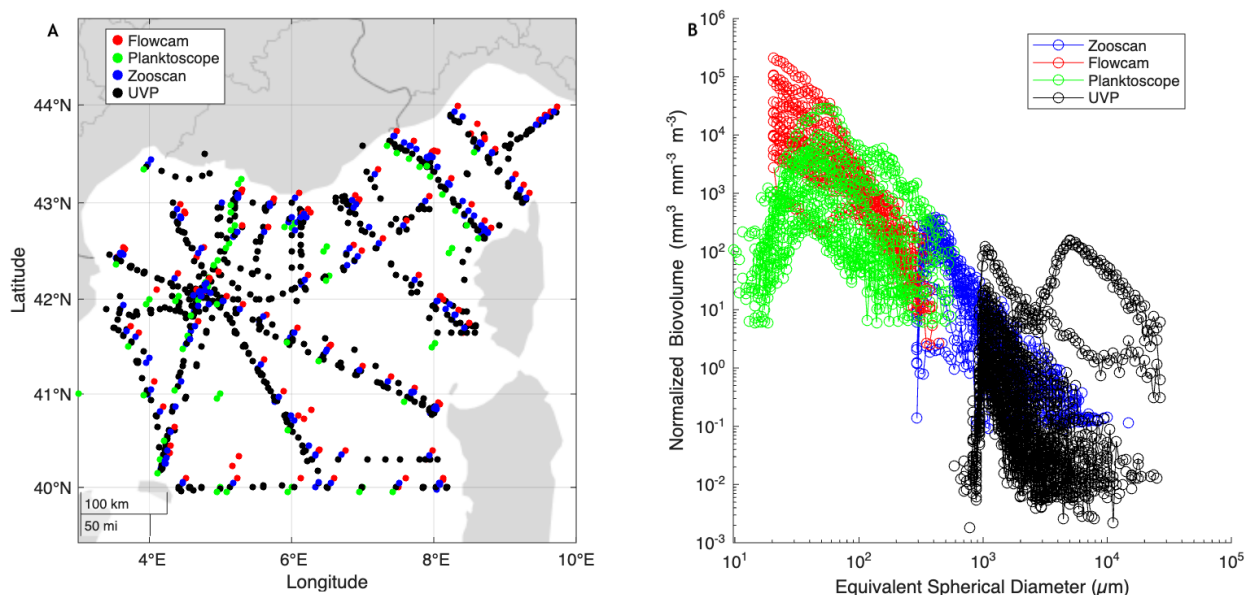


Figure 7: A) Localisation of the different samples obtained and covering the size spectra of living organisms from microplankton (Flowcam, Planktoscope), mesozooplankton (WP2 nets analysed through Zooscan) and macrozooplankton and marine snow particles observed in-situ through profiling camera (UVP). B) Comparison of the normalized size spectra of living organisms obtained with the different devices during the MOOSE-GE 2024 cruise, demonstrating the complementarity of instruments in capturing the continuum of life forms.



1071 References

- 1072 Aminot, A., K erouel, R., 2007. Dosage automatique des nutriments dans les eaux marines : m ethodes en flux continu.
1073 Ed. Ifremer, M ethodes d'analyse en milieu marin 188 pp
- 1074 Belgacem, M., Schroeder, K., Barth, A., Troupin, C., Pavoni, B., Raimbault, P., Garcia, N., Borghini, M., and
1075 Chiggiato, J.: Climatological distribution of dissolved inorganic nutrients in the western Mediterranean Sea (1981–
1076 2017), *Earth Syst. Sci. Data*, 13, 5915–5949, <https://doi.org/10.5194/essd-13-5915-2021>, 2021.
- 1077 Bethoux, J., Gentili, B., Raunet, J. *et al.* Warming trend in the western Mediterranean deep water. *Nature* 347, 660–
1078 662 (1990). <https://doi.org/10.1038/347660a0>
- 1079 Beuvier, J., B eranger, K., Lebeau-pin Brossier, C., Somot, S., Sevault, F., Drillet, Y., Bourdall e-Badie, R., Ferry, N.,
1080 & Lyard, F. (2012). Spreading of the Western Mediterranean Deep Water after winter 2005: Time scales and deep
1081 cyclone transport. *Journal of Geophysical Research*, 117, C07022. <https://doi.org/10.1029/2011JC007679>
- 1082 Bittig, H. C., K ortzinger, A., Neill, C., van Ooijen, E., Plant, J. N., Hahn, J., Johnson, K. S., Yang, B., and Emerson,
1083 S. R. (2018). Oxygen Optode Sensors: Principle, Characterization, Calibration, and Application in the Ocean.
1084 *Frontiers in Marine Science*, 4:429. <https://doi.org/10.3389/fmars.2017.00429>
- 1085 Bosse, A., Testor, P., Houpert, L., Damien, P., Prieur, L., Hayes, D., Taillandier, V., Durrieu de Madron, X.,
1086 D'Ortenzio, F., Coppola, L., Karstensen, J., and Mortier, L. (2016). Scales and dynamics of submesoscale coherent
1087 vortices formed by deep convection in the northwestern Mediterranean Sea. *Journal of Geophysical Research:*
1088 *Oceans*, 121(10), 7716–7742. <https://doi.org/10.1002/2016JC012144>
- 1089 Bosse A., Julien Lenne, Pierre Testor, Dominique Lef evre, Xavier Durrieu de Madron. Warming of Western Med.
1090 Deep Water in the context of halted deep convection. CIESM 2024, Oct 2024, Palerme, Italy. Hal-04798803
- 1091 Bosse Anthony, Testor Pierre, Coppola Laurent, Bretel Patrice, Dausse Denis, Durrieu De Madron Xavier, Houpert
1092 Lo ic, Labaste Matthieu, Legoff Herv e, Mortier Laurent, D'ortenzio Fabrizio (2025). LION observatory data.
1093 SEANOE. <https://doi.org/10.17882/44411>
- 1094 Bosse Anthony, Bretel Patrice, Le Goff Herv e, Testor Pierre (2024). MOOSE-GE cruises: lowered and ship ADCP
1095 data. SEANOE. <https://doi.org/10.17882/99825>
- 1096 Clayton, T. D., and Byrne, R. H. (1993). Spectrophotometric seawater pH measurements: total hydrogen ion
1097 concentration scale calibration of m-cresol purple and at-sea results. *Deep-Sea Research Part I*, 40(10), 2115–2129.
1098 [https://doi.org/10.1016/0967-0637\(93\)90048-8](https://doi.org/10.1016/0967-0637(93)90048-8)
- 1099 Cocquempot, L., Delacourt, C., Paillet, J., Riou, P., Aucan, J., Castelle, B., Charria, G., Claudet, J., Conan, P.,
1100 Coppola, L., Hocd e, R., Planes, S., Raimbault, P., Savoye, N., Testut, L., and Vuillemin, R. (2019). Coastal Ocean
1101 and Nearshore Observation: A French Case Study. *Frontiers in Marine Science*, 6:324.
1102 <https://doi.org/10.3389/fmars.2019.00324>
- 1103 Conan, P., Testor, P., Estournel, C., D'Ortenzio, F., and Pujo-Pay, M. (2018). Preface to the Special Section: Dense
1104 Water Formations in the Northwestern Mediterranean: From the Physical Forcings to the Biogeochemical
1105 Consequences. *Journal of Geophysical Research: Oceans*, 123(10), 6749–6751.
1106 <https://doi.org/10.1029/2018JC014301>



- 1107 Coppola, L., Prieur, L., Taupier-Letage, I., Estournel, C., Testor, P., Lefèvre, D., Belamari, S., LeReste, S., and
1108 Taillandier, V. (2017). Observation of oxygen ventilation into deep waters through targeted deployment of multiple
1109 Argo-O2 floats in the north-western Mediterranean Sea in 2013. *Journal of Geophysical Research: Oceans*, 122(8),
1110 6325–6341. <https://doi.org/10.1002/2016JC012594>
- 1111 Coppola, L., Legendre, D., Lefevre, L., Prieur, V., Taillandier, and E. Diamond Riquier (2018), Seasonal and inter-
1112 annual variations of dissolved oxygen in the northwestern Mediterranean Sea (DYFAMED site), *Progress in*
1113 *Oceanography*, 162, 187-201, doi:10.1016/j.pocean.2018.03.001.
- 1114 Coppola Laurent, Diamond Riquier Emilie, Carval Thierry, Irisson Jean-Olivier, Desnos Corinne (2025). Dyfamed
1115 observatory data. SEANO. <https://doi.org/10.17882/43749>
- 1116 Coppola, L., P. Raimbault, L. Mortier, and P. Testor (2019), Monitoring the environment in the northwestern
1117 Mediterranean Sea, *Eos*, 100, <https://doi.org/10.1029/2019EO125951>. Published on 25 July 2019.
- 1118 Coppola L., Boutin J., Gattuso J.-P., Lefèvre D. & Metzl N. (2020). The carbonate system in the Ligurian Sea. In:
1119 Migon C., Nival P. & Sciandra A. (Eds.), *The Mediterranean Sea in the era of global change (volume 1) - Evidence*
1120 *from 30 years of multidisciplinary study of the Ligurian sea*, pp. 79-104. London: ISTE Science Publishing LTD.
1121 <https://doi.org/10.1002/9781119706960.ch4>
- 1122 Darmaraki S., Somot S., Sevault F., Nabat P., Cabos W., Cavicchia L., Djurdjevic V., Li L., Sannino G., Sein D.
1123 (2019) Future evolution of Marine Heat Waves in the Mediterranean Sea. *Climate Dynamics*, 53 (3-4):1371-1392,
1124 doi: 10.1007/s00382-019-04661-z
- 1125 Dimier Céline, Ras Joséphine, Claustre Hervé, Uitz Julia (2024). MOOSE_GE cruises: phytoplankton pigments.
1126 SEANO. <https://doi.org/10.17882/99865>
- 1127 Dickson et al., 2007: Dickson, A.G., Sabine, C.L., and Christian, J.R. (Eds.) (2007). Guide to best practices for ocean
1128 CO₂ measurements. PICES Special Publication 3, 191 pp. <https://doi.org/10.25607/OBP-1342>
- 1129 Dickson and Goyet, 1994: Dickson, A.G., and Goyet, C. (Eds.) (1994). Handbook of methods for the analysis of the
1130 various parameters of the carbon dioxide system in sea water. Version 2. ORNL/CDIAC-74, Oak Ridge National
1131 Laboratory, Oak Ridge, Tennessee, 198 pp. <https://doi.org/10.2172/10107773>
- 1132 Doney et al., 2009: Doney, S.C., Fabry, V.J., Feely, R.A., and Kleypas, J.A. (2009). Ocean acidification: The other
1133 CO₂ problem. *Annual Review of Marine Science*, 1, 169–192.
1134 <https://doi.org/10.1146/annurev.marine.010908.163834>
- 1135 D'Ortenzio & d'Alcalà, 2009: D'Ortenzio, F., and Ribera d'Alcalà, M. (2009). On the trophic regimes of the
1136 Mediterranean Sea: a satellite analysis. *Biogeosciences*, 6, 139–148. <https://doi.org/10.5194/bg-6-139-2009>
- 1137 Durrieu De Madron Xavier, Heussner Serge, Delsaut Nicole, Kunesch Stéphane, Menniti Christophe
1138 (2024). BILLION observatory data. SEANO. <https://doi.org/10.17882/45980>
- 1139 Durrieu de Madron X. L. Houpert P. Puig A. Sanchez-Vidal P. Testor A. Bosse C. Estournel S. Somot F. Bourrin M.
1140 N. Bouin M. Beauverger L. Beguery A. Calafat M. Canals C. Cassou L. Coppola D. Dausse F. D'Ortenzio J. Font S.
1141 Heussner S. Kunesch D. Lefevre H. Le Goff J. Martín L. Mortier A. Palanques P. Raimbault (2013), Interaction of
1142 dense shelf water cascading and open-sea convection in the northwestern Mediterranean during winter 2012,
1143 *Geophysical Research Letters*, 40(7), 1379-1385, doi:10.1002/grl.50331.



- 1144 Durrieu de Madron X., S. Ramondenc, L. Berline, Loïc Houpert, Anthony Bosse, et al.. Deep sediment resuspension
1145 and thick nepheloid layer generation by open-ocean convection. *J.Geophys.Res.Oceans*, 2017, 122 (3), pp.2291-
1146 2318. [10.1002/2016jc012062](https://doi.org/10.1002/2016jc012062)
- 1147 Edmond, 1970: Edmond, J.M. (1970). High precision determination of titration alkalinity and total carbon dioxide
1148 content of sea water by potentiometric titration. *Deep-Sea Research*, 17(4), 737–750. [https://doi.org/10.1016/0011-
1149 7471\(70\)90038-0](https://doi.org/10.1016/0011-7471(70)90038-0)
- 1150 Escudier, R., Renault, L., Pascual, A., Brasseur, P., Chelton, D., & Beuvier, J. (2016). Eddy properties in the Western
1151 Mediterranean Sea from satellite altimetry and a numerical simulation. *Journal of Geophysical Research: Oceans*,
1152 121, 3990–4006. <https://doi.org/10.1002/2015JC011371>
- 1153 Estournel, C., P. Testor, P. Damien, F. D’Ortenzio, P. Marsaleix, P. Conan, F. Kessouri, X. Durrieu de Madron, L.
1154 Coppola, J-M. Lellouche, S. Belamari, L. Mortier, C. Ulses, M-N. Bouin, L. Prieur (2016b), High resolution
1155 modeling of dense water formation in the north-western Mediterranean during winter 2012-2013: Processes and
1156 budget, *Journal of Geophysical Research-Oceans*, 121(7), 5367-5392, doi:10.1002/2016jc011935.
- 1157 Feliu, thèse 2020: Feliu, G. (2020). Étude de la structure communautaire et du rôle trophique du mésozooplancton
1158 en Méditerranée lors de deux campagnes océanographiques de grande échelle PEACETIME et MOOSE en 2017.
1159 Thèse de doctorat, Aix-Marseille Université.
- 1160 Fourier M, Coppola L, Claustre H, D’Ortenzio F, Sauzède R and Gattuso J-P (2020) A Regional Neural Network
1161 Approach to Estimate Water-Column Nutrient Concentrations and Carbonate System Variables in the Mediterranean
1162 Sea: CANYON-MED. *Front. Mar. Sci.* 7:620. doi: 10.3389/fmars.2020.00620
- 1163 Fourier, M., Coppola, L., D’Ortenzio, F., Migon, C., & Gattuso, J.-P. (2022). Impact of intermittent convection in
1164 the northwestern Mediterranean Sea on oxygen content, nutrients, and the carbonate system. *Journal of Geophysical
1165 Research: Oceans*, 127, e2022JC018615.
- 1166 Giorgi, F., 2006. Climate change hot-spots. *Geophysical Research Letters*, 33, L08707.
1167 <https://doi.org/10.1029/2006GL025734>
- 1168 Harris, R., Wiebe, P., Lenz, J., Skjoldal, H.R., and Huntley, M. (2000). *ICES Zooplankton Methodology Manual*.
1169 Elsevier Science.
- 1170 Herrmann, M., Auger, P.-A., Ulses, C., and Estournel, C. (2017). Long-term monitoring of ocean deep convection
1171 using multisensors altimetry and ocean color satellite data. *Journal of Geophysical Research: Oceans* 122, 1457-
1172 1475.
- 1173 Heimbürger, L.-E., H. Lavigne, C. Migon, F. D’Ortenzio, C. Estournel, L. Coppola, and J.-C. Miquel (2013),
1174 Temporal variability of vertical export flux at the DYFAMED time-series station (Northwestern Mediterranean Sea),
1175 *Progress in Oceanography*, 119, 59-67, doi:10.1016/j.pocean.2013.08.005.
- 1176 Holmes R.M., Aminot A., Kérouel R., Hoker B.A., Peterson B.J., 1999. *Can. J. Fish. Aquat. Sci.*, 56(10), 1801-1808
- 1177 Houpert, L., X. Durrieu de Madron, P. Testor, A. Bosse, F. D’Ortenzio, M-N. Bouin, D. Dausse, H. Le Goff, S.
1178 Kunesch, M. Labaste, L. Coppola, L. Mortier, P. Raimbault (2016), Observations of open-ocean deep convection in
1179 the northwestern Mediterranean Sea: Seasonal and interannual variability of mixing and deep water masses for the
1180 2007-2013 Period, *Journal of Geophysical Research-Oceans*, 121(11), 8139-8171, doi:10.1002/2016jc011857.
- 1181 IPCC (2022). *Climate Change 2022 - Mitigation of Climate Change*.



- 1182 Irisson J-O., Laurent Salinas, Sebastien Colin, Team Complex, Marc Picheral. EcoTaxa: a tool to support the
1183 taxonomic classification of large datasets through supervised machine learning. *SFEcologie 2022*, 2022, Metz,
1184 France
- 1185 Jalabert, L., Elineau, A., Brandão, M., & Picheral, M. (2025a). Zooscan-Zooprocess user manual and procedures at
1186 the Quantitative Imaging Platform of Villefranche-sur-Mer (PIQv) (1.3). Zenodo.
1187 <https://doi.org/10.5281/zenodo.15114134>
- 1188 Jalabert, L., Lombard, F., & Picheral, M. (2025b). FlowCam Zooprocess user manual and procedures at the
1189 Quantitative Imaging Platform of Villefranche sur Mer (PIQv). Zenodo. <https://doi.org/10.5281/zenodo.15113735>
- 1190 Josey, S. A. & Schroeder, K. (2023). Declining winter heat loss threatens continuing ocean convection at a
1191 Mediterranean dense water formation site. *Environmental Research Letters*, 18(2), 024005.
1192 <https://doi.org/10.1088/1748-9326/aca9e4>
- 1193 Kessouri, Fayçal, Caroline Ulses, Claude Estournel, Patrick Marsaleix, Tatiana Severin, Mireille Pujó-Pay, Jocelyne
1194 Caparros, Patrick Raimbault, Orens Pasqueron de Fommervault, Fabrizio D'Ortenzio, Vincent Taillandier, Pierre
1195 Testor, Pascal Conan, (2017). Nitrogen and phosphorus budgets in the Northwestern Mediterranean deep convection
1196 region. *Journal of Geophysical Research: Oceans*. <http://dx.doi.org/10.1002/2016JC012665>
- 1197 Kessouri, F., Ulses, C., Estournel, C., Marsaleix, P., D'Ortenzio, F., Severin, T., et al. (2018). Vertical mixing effects
1198 on phytoplankton dynamics and organic carbon export in the western Mediterranean Sea. *Journal of Geophysical*
1199 *Research: Oceans*, 123. <https://doi.org/10.1002/2016JC012669>
- 1200 Krahnemann, G., and Schott, F. (1998). Longterm increases in Western Mediterranean salinities and temperatures:
1201 Anthropogenic and climatic sources. *Geophysical Research Letters* 25, 4209-4212.
- 1202 Krom, M.D., Herut, B. and Mantoura, R.F.C. (2004) Nutrient budget for the Eastern Mediterranean: Implications for
1203 phosphorus limitation. *Limnology and Oceanography*, 49 (5). pp. 1582-1592. ISSN 0024-3590
- 1204 Lejeusne, C., Chevaldonne, P., Pergent-Martini, C., Boudouresque, C.F., and Perez, T. (2010). Climate change
1205 effects on a miniature ocean: the highly diverse, highly impacted Mediterranean Sea. *Trends Ecol Evol* 25, 250-260.
- 1206 Margirier, F., Testor, P., Heslop, E., Mallil, K., Bosse, A., Houpert, L., Mortier, L., Bouin, M.N., Coppola, L.,
1207 D'ortenzio, F., Durrieu De Madron, X., Mourre, B., Prieur, L., Raimbault, P., and Taillandier, V. (2020). Abrupt
1208 warming and salinification of intermediate waters interplays with decline of deep convection in the Northwestern
1209 Mediterranean Sea. *Sci Rep* 10, 20923.
- 1210 Marsaleix P., Auclair F., Floor J. W., Herrmann M. J., Estournel C., Pairaud I., Ulses C., 2008. Energy conservation
1211 issues in sigma-coordinate free-surface ocean models. *Ocean Modelling*. 20, 61-89.
1212 <http://dx.doi.org/10.1016/j.ocemod.2007.07.005>
- 1213 Medecc (2020). "Climate and Environmental Change in the Mediterranean Basin – Current Situation and Risks for
1214 the Future", in: *First Mediterranean Assessment Report (Version 1)*.
- 1215 Merlivat, L., Boutin, J., Antoine, D., et al., 2018. Increase of dissolved inorganic carbon in the Mediterranean Sea.
1216 *Biogeosciences*, 15, 5653–5674. <https://doi.org/10.5194/bg-15-5653-2018>
- 1217 MerMex Group, 2011. Marine ecosystems' responses to climatic and anthropogenic forcings in the Mediterranean.
1218 *Progress in Oceanography*, 91(2), 97–166. <https://doi.org/10.1016/j.pocean.2011.02.003>



- 1219 Metzl Nicolas, Fin Jonathan, Lo Monaco Claire, Mignon Claude, Alliouane Samir, Antoine David, Bourdin
1220 Guillaume, Boutin Jacqueline, Bozec Yann, Conan Pascal, Coppola Laurent, Diaz Frédéric, Douville Eric, Durrieu
1221 de Madron Xavier, Gattuso Jean-Pierre, Gazeau Frédéric, Golbol Melek, Lansard Bruno, Lefèvre Dominique,
1222 Lefèvre Nathalie, Lombard Fabien, Louanchi Ferial, Merlivat Liliane, Olivier Léa, Petrenko Anne, Petton Sébastien,
1223 Pujon-Pay Mireille, Rabouille Christophe, Reverdin Gilles, Ridame Céline, Tribollet Aline, Vellucci Vincenzo,
1224 Wagener Thibaut, Wimart-Rousseau Cathy (2024). A synthesis of ocean total alkalinity and dissolved inorganic
1225 carbon measurements from 1993 to 2022: the SNAPO-CO2-v1 dataset. Earth System Science Data, 16, 89-120.
1226 Publisher's official version : <https://doi.org/10.5194/essd-16-89-2024>
- 1227 Millot, C., 1999. Circulation in the Western Mediterranean Sea. Journal of Marine Systems, 20, 423–442.
1228 [https://doi.org/10.1016/S0924-7963\(98\)00078-5](https://doi.org/10.1016/S0924-7963(98)00078-5)
- 1229 Miquel, J.-C., Martin, J., Gasser, B., et al., 2011. Dynamics of particle fluxes in the open northwestern Mediterranean
1230 Sea. Progress in Oceanography, 91, 461–481. <https://doi.org/10.1016/j.pocean.2011.07.020>
- 1231 Mourre B, Clementi E, Coppini G, Coppola L, Korres G, Novellino A, Álvarez-Fanjul E, Daniel P, Zodiatis G,
1232 Schroeder K, Tintore J (2023) Chapter 10 - Mediterranean observing and forecasting systems. Oceanography of the
1233 Mediterranean Sea, In: Schroeder K, Chiggiato J (eds), Elsevier, , 335-386 | doi: 10.1016/B978-0-12-823692-
1234 5.00001-7
- 1235 Orr, J.C., Fabry, V.J., Aumont, O., et al., 2005. Anthropogenic ocean acidification over the twenty-first century.
1236 Nature, 437, 681–686. <https://doi.org/10.1038/nature04095>
- 1237 Pasqueron de Fommervault, O., C. Migon, F. D’Ortenzio, M. Ribera d’Alcalà, and L. Coppola (2015), Temporal
1238 variability of nutrient concentrations in the northwestern Mediterranean sea (DYFAMED time-series station), Deep
1239 Sea Research Part I: Oceanographic Research Papers, 100, 1-12, doi:10.1016/j.dsr.2015.02.006.
- 1240 Pearlman J, Bushnell M, Coppola L. et al. (2019) Evolving and Sustaining Ocean Best Practices and Standards for
1241 the Next Decade. *Front. Mar. Sci.* 6:277. doi: 10.3389/fmars.2019.00277
- 1242 Perez, F.F., et al., 2011. The carbon budget of the Mediterranean Sea. Biogeosciences, 8, 1161–1174.
1243 <https://doi.org/10.5194/bg-8-1161-2011>
- 1244 Perruchon A., Hugo Zaccomer, Lombard Fabien 2025. PlanktoScope protocol for plankton imaging. protocols.io
1245 <https://dx.doi.org/10.17504/protocols.io.bp216bq3zggq/v5>
- 1246 Picheral, M., Guidi, L., Stemmann, L., et al., 2010. The Underwater Vision Profiler 5: an advanced instrument for
1247 high spatial resolution studies of plankton and particles. Limnology and Oceanography: Methods, 8, 462–473.
1248 <https://doi.org/10.4319/lom.2010.8.462>
- 1249 Picheral, M., Colin, S. & Irsson, J.-O., 2017. EcoTaxa, a tool for the taxonomic classification of images. Methods
1250 in Oceanography, 20, 1–10. <https://doi.org/10.1016/j.mio.2017.03.003>
- 1251 Picheral, M., & Mériguet, Z. (2025). Description of the metadata and data issued from the Zooprocess and UVPapp
1252 applications and imported or exported from the Ecotaxa application. Zenodo.
1253 <https://doi.org/10.5281/zenodo.15827159>
- 1254 Raimbault P., Neveux J., Lantoiné F., 2004. Oceanis, 30(2) : 189-205
- 1255 Ruti PM, Somot S, Giorgi F, Dubois C, Flaounas E, Obermann A, Dell’Aquila A, Pisacane G, Harzallah A, Lombardi
1256 E, Ahrens B, Akhtar N, Alias A, Arsouze T, Aznar R, Bastin S, Bartholy J, Béranger K, Beuvier J, Bouffies-Cloché



- 1257 S, Brauch J, Cabos W, Calmanti S, Calvet J-C, Carillo A, Conte D, Coppola E, Djurdjevic V, Drobinski P, Elizalde-
1258 Arellano A, Gaertner M, Galàn P, Gallardo C, Gualdi S, Goncalves M, Jorba O, Jordà G, L'Heveder B, Lebeau-pin-
1259 Brossier C, Li L, Liguori G, Lionello P, Maciàs D, Nabat P, Onol B, Raikovic B, Ramage K, Sevault F, Sannino G,
1260 Struglia MV, Sanna A, Torma C, Vervatis V (2016) MED-CORDEX initiative for Mediterranean Climate studies.
1261 Bull. Amer. Meteor. Soc., 97(7), 1187-1208, July 2016, doi: <http://dx.doi.org/10.1175/BAMS-D-14-00176.1>
- 1262 Schroeder, K. *et al.* Abrupt climate shift in the Western Mediterranean Sea. *Sci. Rep.* 6, 23009; doi:
1263 10.1038/srep23009 (2016).
- 1264 Schroeder, K., Chiggiato, J., Bryden, H. L., Borghini, M., & Ben Ismail, S. (2017). Abrupt climate shift in the
1265 Western Mediterranean Sea. *Scientific Reports*, 7, 41721. <https://doi.org/10.1038/s41598-017-04455-5>
- 1266 Sempéré, R., Charrière, B., Van Wambeke, F., et al., 2018. Carbon and nutrient dynamics in the Mediterranean Sea.
1267 *Biogeosciences*, 15, 451–472. <https://doi.org/10.5194/bg-15-451-2018>
- 1268 Send, U., Font, J., Krahnmann, G., et al., 1999. Recent advances in observing the physical oceanography of the
1269 Mediterranean Sea. *Progress in Oceanography*, 44, 37–64. [https://doi.org/10.1016/S0079-6611\(99\)00019-0](https://doi.org/10.1016/S0079-6611(99)00019-0)
- 1270 Somot, S., Sevault, F. & Déqué, M. Transient climate change scenario simulation of the Mediterranean Sea for the
1271 twenty-first century using a high-resolution ocean circulation model. *Clim Dyn* 27, 851–879 (2006).
1272 <https://doi.org/10.1007/s00382-006-0167-z>
- 1273 Somot S., Houpert L., Sevault F., Testor P., Bosse A., Taupier-Letage I., Bouin M.N., Waldman R., Cassou C.,
1274 Sanchez-Gomez E., Durrieu de Madron X., Adloff F., Nabat P., Herrmann M. (2018) Characterizing, modelling and
1275 understanding the climate variability of the deep water formation in the North-Western Mediterranean Sea. *Climate*
1276 *Dynamics*, 51(3), 1179-1210, doi: 10.1007/s00382-016-3295-0
- 1277 Soto-Navarro J., Jordà G., Amores A., Cabos W., Somot S., Sevault F., Maciàs D., Djurdjevic V., Sannino G., Li L.,
1278 Sein D. (2020) Evolution of Mediterranean Sea water properties under climate change scenarios in the Med-
1279 CORDEX ensemble. *Clim. Dyn.* 54, 2135–2165, <https://doi.org/10.1007/s00382-019-05105-4>
- 1280 Stabholz M., Xavier Durrieu de Madron, Miquel Canals, A. Khripounoff, Isabelle Taupier-Letage, et al.. Impact
1281 of open-ocean convection on particle fluxes and sediment dynamics in the deep margin of the Gulf of Lions.
1282 *Biogeosciences*, 2013, 10 (2), pp.1097-1116. (10.5194/BG-10-1097-2013).
- 1283 Tanhua, T., Hainbucher, D., Schroeder, K., et al., 2015. Ventilation and anthropogenic carbon in the Mediterranean
1284 Sea. *Biogeosciences*, 12, 507–525. <https://doi.org/10.5194/bg-12-507-2015>
- 1285 Testor Pierre, Bosse Anthony, Coppola Laurent (2010) MOOSE-GE. SISMER. <https://doi.org/10.18142/235>
- 1286 Testor, P., et al., 2010. Gliders as a component of future observing systems. *Oceanography*, 23(3), 104–115.
1287 <https://doi.org/10.5670/oceanog.2010.04>
- 1288 Testor P., Bosse A., Houpert L., Margirier F., Mortier L., Lego H., Dausse D., Labaste M., Karstensen J., Hayes D.,
1289 Olita A., Ribotti A., Schroeder K., Chiggiato J., Onken R., Heslop E., Mourre B., D'Ortenzio F., Mayot N., Lavigne
1290 H., de Fommervault O., Coppola L., Prieur L., Taillandier V., Durrieu de Madron X., Bourrin F., Many G., Damien
1291 P., Estournel C., Marsaleix P., Taupier-Letage I., Raimbault P. Waldman R., Bouin M.-N., Giordani H., Caniaux G.,
1292 Somot S., Ducrocq V., Conan P. (2018) Multiscale observations of deep convection in the northwestern
1293 Mediterranean Sea during winter 2012-2013 using multiple platforms. *JGR-Oceans*, 123(3), 1745-1776,
1294 doi:10.1002/2016JC012671, Special Issue HyMeX-Mermex



- 1295 Tintoré J, Pinardi N, et al. (2019) Challenges for Sustained Observing and Forecasting Systems in the Mediterranean
1296 Sea. *Front. Mar. Sci.* 6:568. doi: 10.3389/fmars.2019.00568
- 1297 Ulses, C., Estournel, C., Fourier, M., Coppola, L., Kessouri, F., Lefèvre, D., and Marsaleix, P.: Oxygen budget of
1298 the north-western Mediterranean deep- convection region, *Biogeosciences*, 18, 937–960, [https://doi.org/10.5194/bg-](https://doi.org/10.5194/bg-18-937-2021)
1299 18-937-2021, 2021.
- 1300 Ulses, C., Estournel, C., Marsaleix, P., Soetaert, K., Fourier, M., Coppola, L., Lefèvre, D., Touratier, F., Goyet, C.,
1301 Guglielmi, V., Kessouri, F., Testor, P., and Durrieu de Madron, X. (2023) Seasonal dynamics and annual budget of
1302 dissolved inorganic carbon in the northwestern Mediterranean deep-convection region, *Biogeosciences*, 20, 4683–
1303 4710, <https://doi.org/10.5194/bg-20-4683-2023>.
- 1304 Vandromme, P., et al., 2011. Seasonal variability of nutrients in the northwestern Mediterranean. *Journal of Marine*
1305 *Systems*, 87, 136–149. <https://doi.org/10.1016/j.jmarsys.2011.03.003>
- 1306 Vernet, C., Henry, N., Lecubin, J., De Vargas, C., Hingamp, P., and Lescot, M. (2021). The Ocean barcode atlas:
1307 A web service to explore the biodiversity and biogeography of marine organisms. *Mol Ecol Resour* 21, 1347-1358.
- 1308 Waldman R., Somot S., Herrmann M., Testor P., Estournel C., Sevault F., Prieur L., Mortier L., Coppola L.,
1309 Taillandier V., Conan P., Dausse D. (2016) Estimating dense water volume and its evolution for the year 2012-2013
1310 in the North-western Mediterranean Sea: an Observing System Simulation Experiment approach. *JGR-Oceans*,
1311 121(9), 6696-6716, doi: 10.1002/2016JC011694, Special Issue HyMeX-MerMex
- 1312 Waldman R., Somot S., Herrmann M., Bosse A., Caniaux G., Estournel C., Houpert L., Prieur L., Sevault F., Testor
1313 P. (2017) Modelling of the intense 2012-2013 dense water formation event in the northwestern Mediterranean Sea:
1314 Evaluation with an ensemble simulation approach. *J. Geophys. Res. Oceans*, 122, doi:10.1002/2016JC012437,
1315 Special Issue HyMeX-MerMex
- 1316 Waldman R., Brüggemann N., Bosse A., Sevault F., Somot S., Spall M. (2018) Overturning the Mediterranean
1317 Thermohaline Circulation. *GRL*, 45(16):8407-8415, doi: 10.1029/2018GL078502
- 1318 Williams, P.J.leB., and Jenkinson, N.W. (1982). A transportable microprocessor-controlled precise Winkler titration
1319 suitable for field station and shipboard use. *Limnol. Oceanogr.*, 27 (3), 576-584.
- 1320 Wimart-Rousseau C, Wagener T, Bosse A, Raimbault P, Coppola L, Fourier M, Ulses C, Lefèvre D (2023)
1321 Assessing seasonal and interannual changes in carbonate chemistry across two time-series sites in the North Western
1322 Mediterranean Sea. *Front Mar Sci* 10 | doi: [10.3389/fmars.2023.1281003](https://doi.org/10.3389/fmars.2023.1281003)
- 1323 Yao, K.M., Marcou, O., Goyet, C., Guglielmi, V., Touratier, F. & Savy, J.-P., 2016. Time variability of the north-
1324 western Mediterranean Sea pH over 1995-2011. *Marine Environmental Research*, 116, 51–60.
1325 <https://doi.org/10.1016/j.marenvres.2016.02.016>